THE CATALYTIC MECHANISM OF *MYCOBACTERIUM TUBERCULOSIS* CATALASE-PEROXIDASE (KATG) AND ISONIAZID ACTIVATION

by

XIANGBO ZHAO

A dissertation submitted to the Graduate Faculty in Biochemistry in partial fulfillment of the requirements for the degree of Doctor of Philosophy,

The City University of New York

2005

This manuscript has been read and accepted for the Graduate Faculty in Biochemistry in satisfaction of the dissertation requirement for the degree of Doctor of Philosophy.

Date	Chair of Examining Committee Dr. Richard S. Magliozzo
Date	Executive Officer Dr. Lesley Davenport

Supervisory Committee:

Dr. Johannes J.P. Schelvis

Dr. Manfred Philipp

Dr. John S. Blanchard

Dr. Lesley Davenport

The City University of New York

ABSTRACT

THE CATALYTIC MECHANISM OF *MYCOBACTERIUM TUBERCULOSIS* CATALASE-PEROXIDASE (KATG) AND ISONIAZID ACTIVATION

by

Xiangbo Zhao

Adviser: Dr. Richard S. Magliozzo

Mycobacterium tuberculosis catalase-peroxidase (KatG) is a bi-functional heme enzyme and is involved in the *in vivo* activation of the antituberculosis drug isoniazid. The resting enzyme (ferric) is usually activated by peroxide and gives rise to a highly oxidative intermediate. Like other heme peroxidases, the catalytic cycle of this enzyme involves heme-based and amino acid based radical intermediates.

In previous studies, a protein based tyrosyl radical was detected in the reaction of this enzyme with alkyl peroxide. However, the location of the radical forming residue(s) required special efforts to elucidate. In this study, nitric oxide (NO) was used as a radical scavenging reagent to label the tyrosyl radical forming residue(s). Quenching of the tyrosyl radical generated in the presence of NO was shown using electron paramagnetic resonance spectroscopy, and formation of nitrotyrosine was confirmed by proteolytic digestion followed by HPLC analysis of the NO-treated enzyme. Edman sequencing of nitrated peptides showed that only Tyr353 was labeled. In the mutant enzyme KatG[Y353F], which was constructed using site-directed mutagenesis, a tyrosyl radical

was also formed upon turnover with peroxide, but in poor yield compared to wild-type KatG. Thus, we propose that Tyr353 is one of the tyrosyl radical forming site(s) in wild type KatG.

Previous studies did not clarify the oxidants that participate in the KatG-mediated activation of isoniazid. In this study, we mimic the *in vivo* oxidative environment by the generation of a continuous flow of small amounts of hydrogen peroxide enzymatically. For the first time, we demonstrated that hydrogen peroxide is a very effective species that accelerates the activation of isoniazid. We also verified that NAD, rather than NADH, is involved in formation of an important inhibitor molecule specific for the action of the antibiotic. A model of an INH activation mechanism is proposed, and the behavior of the isoniazid resistant KatG[S315T] mutant fits this model very well.

ACKNOWLEDGMENTS

I would like to express my sincere gratitude to all those who helped me to finish my thesis. In particular, I am grateful to my mentor, Professor Richard Magliozzo for his tremendous support during the last five years. I have been not only impressed by the breadth of his knowledge, inspired by his enthusiasm in scientific research, but also amazed by his great personality. I really learned a lot from him and enjoyed the work and life in his laboratory.

Many thanks to the members of my Ph.D. committee who monitored my work and took great effort in reading and providing valuable comments on the draft of this thesis. Professor Manfred Philipp taught me lots of bioinformatics skills that are very helpful in my research as well as in the preparation of this thesis. Professor Lesley Davenport, also the executive officer of the Ph.D. program has given me plenty of academic advice that guided me throughout the graduate life. Professor John Blanchard and Professor Johannes Schelvis are both experts in my research field and have provided me with precious suggestions regarding my research project.

I am deeply indebted to Dr. Shengwei Yu and Dr. Salem Chouchane who have offered me a lot of technical help. I should also thank Dr. Stefania Girotto for her assistance in the EPR experiments. Many thanks to Professor Zhen Huang for his guidance during my research rotation in his lab.

I would like to give my special thanks to my wife Xin Chen whose love, encouragement, and consistent support enabled me to complete this work.

TABLE OF CONTENTS

LIST OF TABLES

LIST OF FIGURES

CHAPTER 1

INTRODUCTION

Tuberculosis (TB) is a resurging disease in industrialized countries and continues to be the most dangerous killer in developing and underdeveloped countries. It has never been eradicated like many other infectious diseases, partially due to the increasing occurrence of drug resistance. Therefore, the elucidation of drug resistance mechanisms will play an essential role in the TB control effort.

Isonicotinic acid hydrazide (isoniazid, INH) is a major anti-TB drug and has been used for decades. The resistance against this antibiotic mainly stems from the mutation of a protein from *M. tuberculosis* itself, a bi-functional enzyme catalase–peroxidase (KatG). INH is a pro-drug and needs *in vivo* activation by the KatG enzyme.

In this study, the major efforts have been devoted to gaining a better understanding of the general catalytic cycle of this enzyme, including identification of the tyrosyl radical forming residues. Also addressed is the mechanism of INH activation by KatG in the presence of hydrogen peroxide.

1.1 Tuberculosis - history and current situation

Tuberculosis is an infectious disease that has plagued human beings for centuries. The earliest TB cases were found in the Egyptian mummies, which can be dated back to

as early as 3400 BC (1,2). In the middle of the 18th century, tuberculosis was the leading cause of human death.

Throughout the past century, tremendous progress has been made in the fight against tuberculosis. TB has been receding steadily in the United States and other industrialized countries since the 1950s. However, in the late 1980s to early 1990s, when most people throughout the industrialized counties thought that TB had disappeared, an unexpected increase in tuberculosis cases was reported in the U.S. and European counties (Figure 1.1). Accordingly, the World Health Organization (WHO) declared a global health emergency in 1993. Unfortunately, this old disease continues to be one of most deadly infectious diseases in the 21st century. According to estimates of the World Health Organization, TB kills over 2 million people each year worldwide, with an annual increase of 8 million new cases (3). About one-third of the world's population is currently infected by the bacterium, *Mycobacterium tuberculosis* that causes TB (4). Furthermore, the dangerous combination of HIV/AIDS and TB together with the emergence of TB strains resistant to major chemotherapeutics could threaten global TB control efforts (5,6). Therefore, the danger of tuberculosis can by no means be underestimated, especially in developing countries, where the public health infrastructure is not fully established. The current situation also highlights the gravity of the scientific research efforts that are related to all aspects of TB control: epidemiology, pathology, vaccine development, drug resistance, new drug screening, etc.

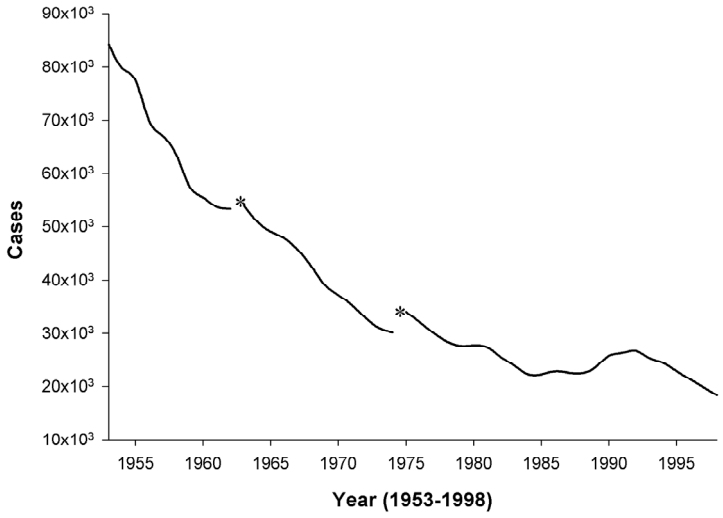

Figure 1.1 Reported tuberculosis cases in the United States. "*" indicates the reporting criteria changes (Source : CDC).

1.2 Treatment of tuberculosis

The treatment of tuberculosis has evolved with human history. In ancient times, treatment mainly involved many superstitious approaches, such as bloodletting, sea voyage, eating boiled crocodile, and "the royal touch". Certainly, those kinds of practices didn't help much to cure this disease.

In 1882, the discovery of *Mycobacterium tuberculosis* by Robert Koch paved the way for systematic tuberculosis research. Thanks to his contribution to discovery of the pathogen, TB vaccine using the attenuated strain known as Bacille Calmette-Guérin (BCG) was subsequently developed in the 1920s (7). Even today, after almost 80 years since its introduction, BCG is still the only TB vaccine available. However, the efficacy of vaccination is quite variable, ranging from <0% to >80% according to meta-analysis

(8). Many scientists now believe that BCG can only protect children from some forms of TB and cannot protect the adult.

The effective chemotherapy of tuberculosis began in the 1940s with the introduction of the broad-spectrum antibiotic, streptomycin. This aminoglycoside interferes with bacterial protein synthesis by binding to the 30S ribosomal subunit. When used alone, streptomycin was found to be very effective against extracellular mycobacteria. However, early in the chemotherapy era, monotherapy with this antibiotic caused significant drug resistance among TB patients (9).

In 1945, Chorine reported that in a murine model of tuberculosis, nicotinamide had antituberculosis activity (10), which contributed to the discovery of the highly specific and potent antituberculosis drug, isoniazid (isonicotinic acid hydrazide, or INH). Further studies have shown that many other nicotinamide analogues, such as ethionamide (ETA) and pyrazinamide (PZA), are also effective chemotherapeutics against TB (Figure 1.2). However, among them, isoniazid is still the most potent one and has been commonly used since 1952 (11).

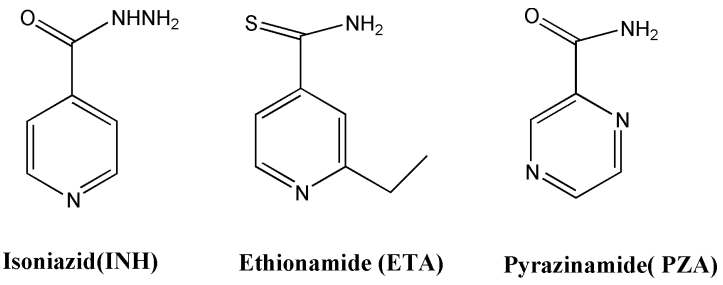

Isoniazid(INH) **Ethionamide (ETA)** **Pyrazinamide(PZA)**

Figure 1.2 Structure of isoniazid and its analogous.

With the discovery of a number of antibiotics, the principles of tuberculosis chemotherapy were established in the mid 1950s. As a result, curative therapy of TB became possible. The introduction of rifampin in the early 1970s further improved the efficiency of chemotherapeutic regimens (12). Since then, the attempt to develop new antituberculosis drugs has been undermined by the growing belief that TB could be conquered in a short time and the prospect of low profits in the drug markets of developed countries where the numbers of TB cases have shrunk steadily.

Antituberculosis drugs fall into three categories, first-line drugs, second-line drugs, and experimental drugs. Isoniazid, ethambutol, rifampin, and streptomycin are among the first-line drugs. Due to the increasing drug resistance, a minimum 6-8 months of administration of a four-drug regimen (isoniazid, rifampicin, pyrazinamide, ethambutol or streptomycin) has been recommended to treat tuberculosis effectively (13). However, over the past decade the widespread INH resistance has hindered the efficacy of this frontline regimen. There is a pressing need for a better understanding of the mechanisms of drug action as well as the origin of drug resistance, which in return will contribute to the discovery of new drugs.

1.3 INH as an antituberculosis agent

Isoniazid (isonicotinic acid hydrazide, INH) was first synthesized by Hans Meyer and Josef Mally in 1912 at German Charles University in Prague. In the early 1950s almost 40 years later, several groups independently demonstrated that INH exhibited potent antituberculosis activity. Since then this antibiotics has been widely used as the

most effective and economical antituberculosis agent (11). However, the mechanism of its action is still under investigation. Initially, several hypotheses had been proposed, including action as an antimetabolite for NAD or pyridoxal phosphate. In the early 1970s, Takayama and colleagues reported that INH could inhibit the *in vivo* synthesis of mycolic acids, long chain fatty acid-containing components of the mycobacterial cell wall, and that the inhibition of mycolic acid biosynthesis correlates with cell death (14,15). Later, Quemard et al. investigated the INH inhibition of mycolic acid synthesis using cell extracts from both INH-sensitive and INH-resistant strains of *Mycobacterium aurum*. They demonstrated that the cell extract of the INH-sensitive strain was inhibited by INH treatment, while the preparation from the INH-resistant strain was not. Furthermore, the inhibition of mycolic acid could not be recovered by adding NAD or pyridoxal phosphate (16). Thus, the effect of INH treatment cannot be simply explained as being due to antimetabolite properties. At present, the well accepted mechanism is that INH treatment disrupts the biosynthesis of mycolic acid in *M. tuberculosis*, which ultimately leads to cell death (17). Even though pyrazinamide (PZA) and INH are analogues of nicotinamide, the proposed mechanisms of their action are quite different (18) (Figure 1.3).

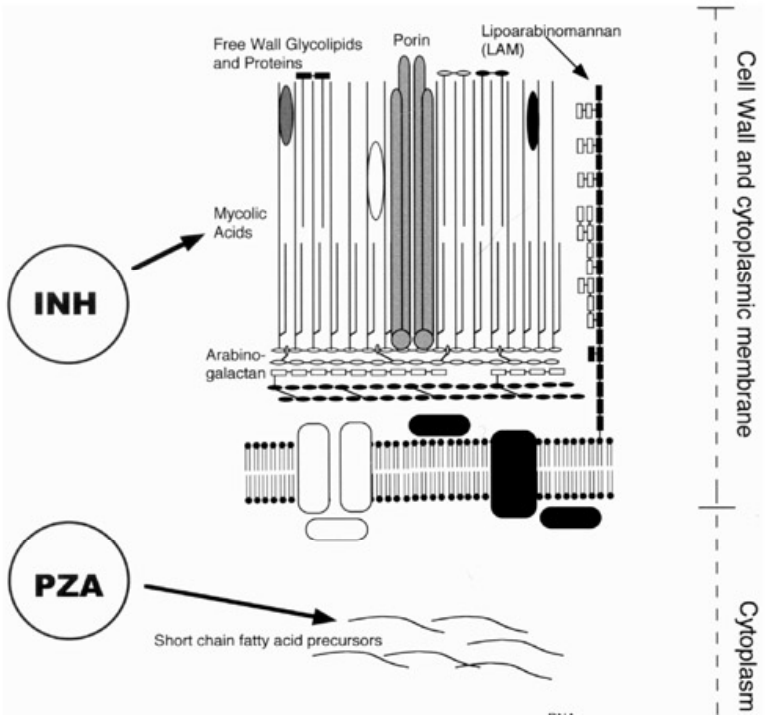

Figure 1.3 Proposed sites of action of isoniazid (INH) and pyrazinamide. INH inhibits the synthesis of mycolic acids; pyrazinamide (PZA) inhibits the synthesis of short-chain fatty acid precursors. This figure is adapted from Somoskovi et al. (18).

The molecular target of INH action in mycobacteria has been very complicated to confirm. Banerjee et al., reported that a missense mutation within the mycobacterial *inhA* gene (a serine residue replaced by alanine: S94A in the enzyme) could confer resistance to both isoniazid and ethionamide in *M. tuberculosis* (19). Later, Quemard and colleagues successfully over-expressed, purified and characterized the protein (InhA) encoded by *M. tuberculosis inhA* gene (20). They have demonstrated that InhA is an enoyl-acyl carrier protein (ACP) reductase involved in the elongation of the long chain fatty acids. Shortly after, the crystal structures of wild type and S94A mutant of InhA were solved (21).

In the continuing effort to confirm the target of INH action in *M. tuberculosis*, mutations in another enzyme, beta-ketoacyl-acyl carrier protein synthase (KasA), which is also involved in the synthesis of fatty acids (22) have been discovered. InhA, KasA, and several other proteins in *Mycobacterium tuberculosis* constitute a unique type II fatty acid synthase system (FAS II) responsible for the production of mycolic acids. Given the fact that mutations could be found in several enzymes in INH resistant isolates, there is still some debate about which enzyme is the primary target of INH (23).

1.4 INH activation and *M. tuberculosis* KatG

INH resistant strains were found in clinical isolates shortly after the introduction of INH as an antituberculosis agent (24,25). It was observed long ago that INH resistance in mycobacteria was often accompanied by reduced levels of catalase/peroxidase activity (25,26). The molecular mechanism underlying this observation was revealed by Zhang and colleagues in 1992. They demonstrated that either deletion or point mutation of the *katG* gene could give rise to INH resistance (27). Later, Zhang and colleagues showed that INH sensitivity could be restored by introduction of the *katG* gene into an INH-resistant, catalase-deficient strain (28). According to the studies by several groups, as much as 50-70% of INH resistant in tuberculosis is due to *katG* mutation (29-33). The most common mutation of *katG*, and the one most referred to, was found within codon 315, leading to replacement of serine by some bulkier residue (Thr or Asn) in INH resistant strains.

Wild type KatG from *M. tuberculosis* as well as specific mutants isolated from INH-resistant stains, have been sequenced, overexpressed and kinetically characterized (34-36). Johnsson and Shultz showed that INH and its metabolites have no significant effect on the peroxidase or catalase activity of KatG (37). Thus, KatG is not a target for INH, but an activator for this drug. Since the inhibition of the synthesis of mycolic acid occurs only in the presence of functional KatG, it is now widely accepted that isoniazid is a pro-drug and its antituberculosis effect requires in vivo activity of KatG, a catalase-peroxidase (20,36,38). Though many bacteria express a catalase-peroxidase, susceptibility to INH varies greatly, from relative resistance in *E. coli* to moderate sensitivity in *M. smegmatis* and very high sensitivity in *M. tuberculosis* (39).

1.5 Structure of *M. tuberculosis* KatG

KatGs, found mostly in bacteria (but also present in fungi and plants) represent a unique category of heme peroxidases that have catalase activity as well as typical peroxidase activity with broad specificity. *M. tuberculosis* KatG monomer, an 80 k-Da protein containing 740 residues, is thought to have evolved from an ancestral prokaryotic peroxidase. This enzyme, like other bacterial KatGs, has little sequence homology with typical catalases (either bacterial or from higher organisms) but possesses high homology (especially at the active site) to yeast cytochrome c peroxidase (CcP) and to other plant peroxidases (40). The peroxidases from plants, fungi and yeast usually contain 290-350 amino acid residues. The approximate doubling of the KatG peptide is thought to have been caused by gene duplication. Although each half of the KatG peptide chain is

homologous to yeast CcP, only the N-terminal half has a functional heme-binding site. In the C-terminal domain, a number of key residues, which are essential for heme binding, are not conserved (41).

Following the successful solution of the 3-dimensional structure of KatG from *H. marismortui,* the crystal structures of KatGs from *Burkholderia pseudomallei* and *M. tuberculosis* have also been determined (42-44). Because of high sequence homology (>55%) among these three enzymes, their 3-dimensional structures are also very similar (Figure 1.4).

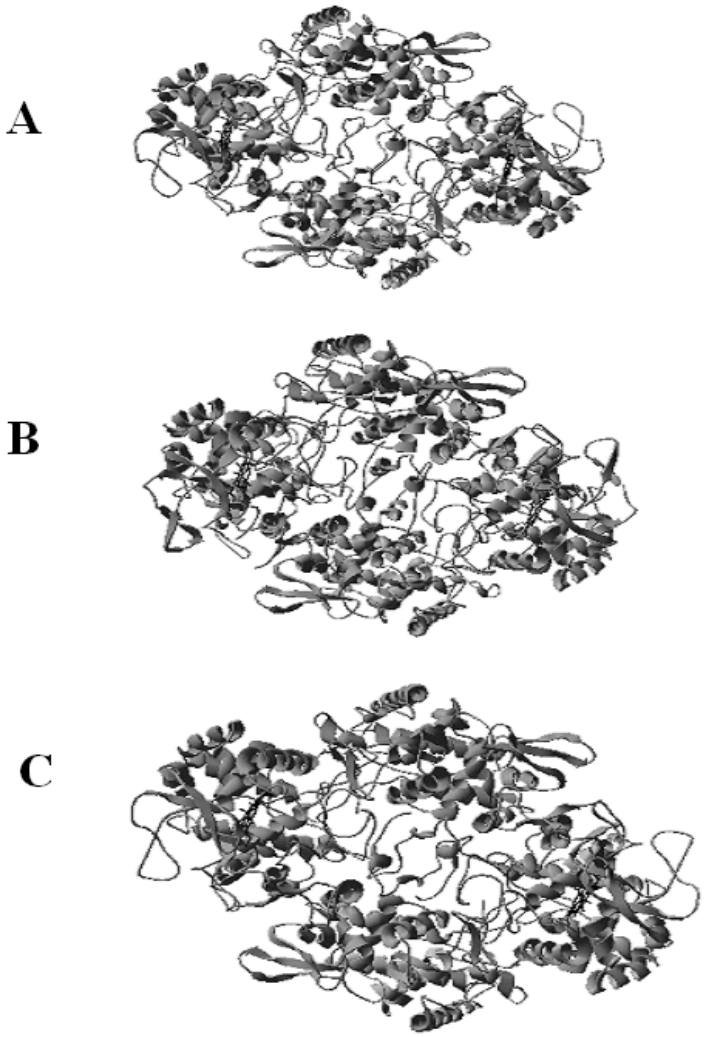

Figure 1.4 Crystal structures of bacterial KatG from various bacteria. A: KatG from *M. tuberculosis* (44); B: KatG from *H. marismortui* (42) ; C: KatG from *B. pseudomallei* (43).

The *M. tuberculosis* KatG crystal consists of two identical subunits with each subunit binding a heme *b* cofactor, which is consistent with the molecular weight of the dimer in solution (34,45). Like other peroxidases, each KatG subunit contains two structurally similar domains and consists mainly of α-helices and very few β-sheets.

The heme group is deeply buried inside the N-terminal domain with a small access channel from the surface. The heme pocket is very hydrophobic with the

exception of a few polar residues thought to be involved in binding the prosthetic group. Six conserved residues (R104, W107, H108, H270, W321, and D381) are seated around the heme site (see Figure 1.5). The crystal structure also showed that the heme iron (Fe^{III}) is bound to five ligands (but not in all cases), with four of them being nitrogen atoms of the heme porphyrin ring, an imidazole side chain of a proximal histidine (H270) acting as the 5th ligand. If we cut the protein along the heme plane, the side with the heme His ligand is called the proximal side, and the other half is called distal side. The linkage between heme iron and proximal histidine is a covalent bond, which can be broken in acidic pH. His270 is a conserved residue that is present in almost all types of peroxidases. The heme porphyrin plane is perpendicular to the imidazole ring. On the distal side, there is another conserved non-coordinated histidine (His108), which is termed the distal histidine.

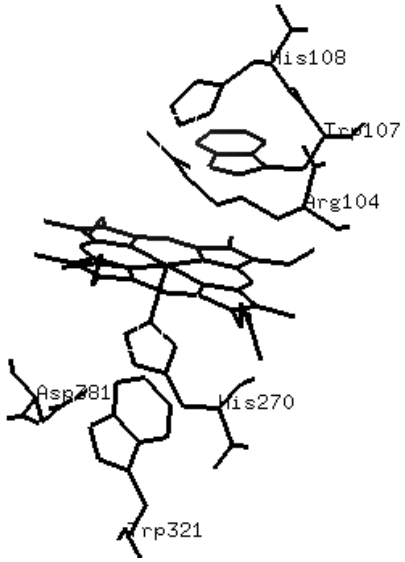

Figure 1.5 Conserved residues at the active site of *M. tuberculosis* KatG. This figure was constructed using Swiss PdbViewer software and *M. tuberculosis* KatG protein data bank file.

In the resting state, the heme iron is five-coordinate in most peroxidases. However, according to electronic absorption and resonance Raman studies, the coordination number in TB KatG can convert to six when the protein has been stored for a few weeks (46) or when it is isolated and purified in amine buffers (such as TEA-HCl). The extra ligand is thought to be a water molecule.

In the *M. tuberculosis* KatG crystal structure, the side chain of tyrosine residue Y229 is covalently linked to two other residues, Met 255 through a carbon sulfur bond, and, to Trp 107 through a carbon-carbon bond (see Figure 1.6). Similarly, the homologous tyrosine, tryptophan, and methionine residues in *B. p*. KatG and *H. m*. KatG were also found covalently linked in their crystal structures (42,43). The unusual three-residue adduct seems to be a general feature of catalase-peroxidases. This adduct was not formed in the crystal preparation step, since it also was also found in the protein before crystallization (47). Studies conducted by several groups showed that KatGs will lose most of their catalase activity when this adduct is disrupted by mutating the key tyrosine (Y229 in *M. tuberculosis*) or either of the other two residues (48-50).

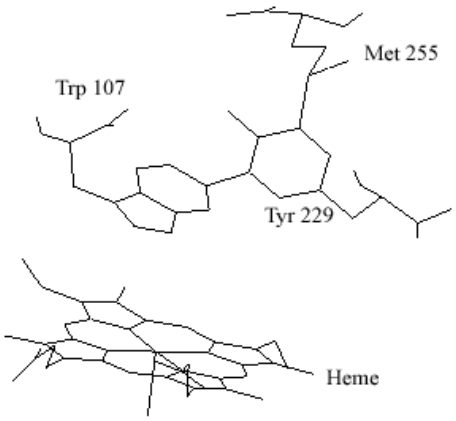

Figure 1.6 The three-amino-acid adduct in *M. tuberculosis* KatG.

1.6 Catalytic functions of *M. tuberculosis* KatG

Oxidation processes can proceed through loss of electrons from a substance either in pairs or by one at a time with a free radical as a transient intermediate. It has been known for a long time that peroxidatic pathway involves single electron oxidation. The reaction mechanisms by which heme peroxidases function have been well characterized in horseradish peroxidase (HRP) and cytochrome c peroxidase. The peroxidase catalytic cycle usually begins with the oxidation of heme by peroxides, which results in the formation of a very reactive intermediate, Compound I (Figure 1.7), an oxyferryl (Fe^{IV}=O) porphyrin cation radical, which is two oxidation equivalents above the Fe^{III} resting state, which is considered to be in a radical cation state. Then, the reduction of Compound I by one electron gives rise to Compound II, another intermediate that contains an oxyferryl heme but with the cation radical reduced back to the resting porphyrin state. This is usually the rate-determining step of the full reaction cycle.

Finally, through another one-electron transfer process, Compound II is reduced to the ferric (Fe^{III}) state, the native enzyme (40,51,52):

Native peroxidase + ROOH → Compound I + ROH

Compound I + AH → Compound II + A•

Compound II + AH → Native peroxidase + A• + H_2O

AH is a reducing substrate, such as a phenol or other electron donor, and A• is the corresponding free radical. After donating one electron, usually through the loss of a hydrogen atom, the reducing substrate becomes a radical species, which is very reactive.

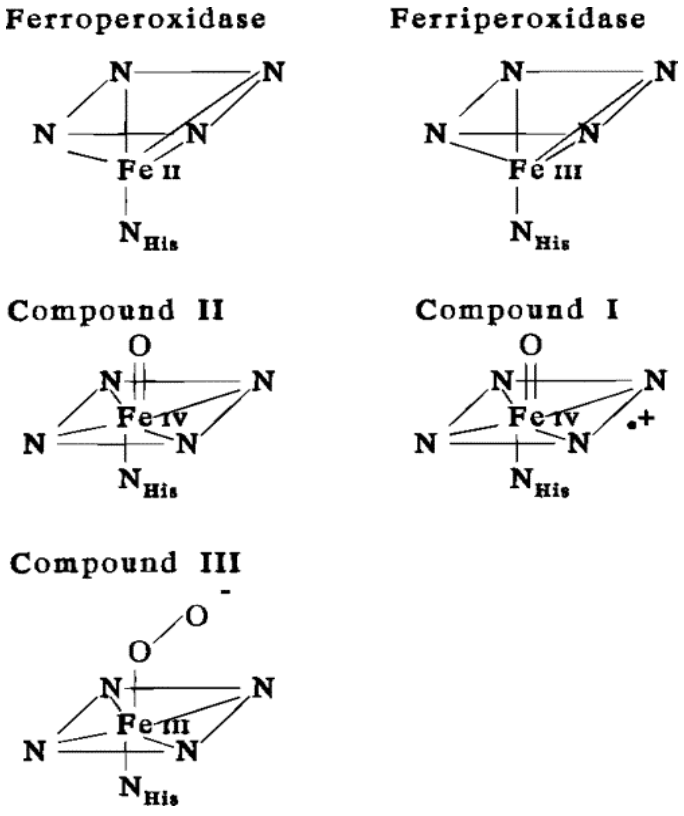

Figure 1.7 Main redox states of peroxidase heme. Adapted from Scheeline et al. (53). Protein structure not shown, and details of heme ring also omitted to emphasize Fe/oxygen structure and free-radical character of Compound I.

The typical catalase reaction cycle starts from the resting enzyme reacting with one molecule of H_2O_2 to produce Compound I. Compound I reacts with a second H_2O_2 molecule transferring the enzyme back to the resting state and one equivalent each of oxygen and water are released:

$$\text{Catalase} + H_2O_2 \rightarrow \text{Compound I} + H_2O$$

$$\text{Compound I} + H_2O_2 \rightarrow \text{Catalase} + O_2 + H_2O$$

Thus, the catalase cycle and peroxidase cycle share the same intermediate, Compound I. However, most peroxidases cannot use H_2O_2 as reducing substrate and thus are not able to act as a catalase. The details of each step of the mechanism are still not clear. As a bi-functional enzyme, *M. tuberculosis* KatG exhibits significant catalase activity as well as typical peroxidase function. This enzyme has a broad range of peroxidatic substrates, including phenolics, pyridines, and amines, etc., and can use hydrogen peroxide and other organic peroxides as oxidants. The catalytic pathway of KatG follows similar pattern of either enzyme as described above depending on what kind of substrate is present.

Because of its importance in the activation of INH, the catalytic function of *M. tuberculosis* KatG has become the topic of extensive investigation. Aside from above described peroxidase and catalase activities, other catalytic functions including manganese dependant peroxidase activity, hydrazinolytic activity, and NADH-oxidase activity of TB KatG have also been reported (54,55). However, these other functions are all likely to be dependent on the peroxidase pathway. The presence of multiple functions associated with a single enzyme has made it even more complicated to elucidate the mechanism of INH activation.

INH can be peroxidized by KatG, with isonicotinamide and isonicotinic acid being the major products. Some reactive drug intermediates, including radical and electrophilic species have been detected (56). An INH-NAD adduct, produced from INH and NAD(H) in the presence of KatG, has been co-crystallized with InhA and structurally characterized by X-ray crystallography (Figure 1.8). This tightly bound adduct inhibits InhA turnover (57). Its inhibitory effect has been recently confirmed by biochemical studies (37,57-59) and details about the mechanism of inhibition have been described. The discovery of this INH-NAD adduct provided molecular evidence about how INH can affect an enzyme involved in mycolic acid synthesis.

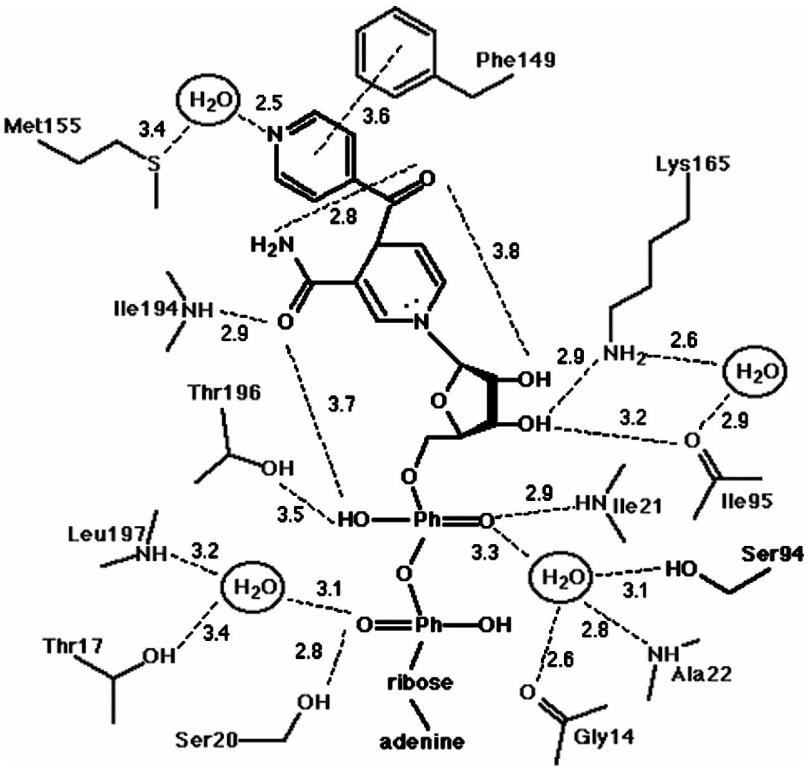

Figure 1.8 Crystal structure of INH-NAD adduct bound to InhA.
Adapted from Rozwarski et al. (57).

1.7 Optical spectra of *M. tuberculosis* KatG

Due to the presence of the iron-protoporphyrin IX co-factor (Figure 1.9), heme proteins and enzymes exhibit optical features that have been the subject of extensive spectroscopic studies. The KatG absorption bands in the visible and near ultraviolet (Soret) region originate from the *d* electrons of iron and the π electrons of the porphyrin ring. The oxidation and spin states of iron and porphyrin and the further interaction between metal and the ligands give rise to multiple absorption bands in the optical spectra of heme proteins.

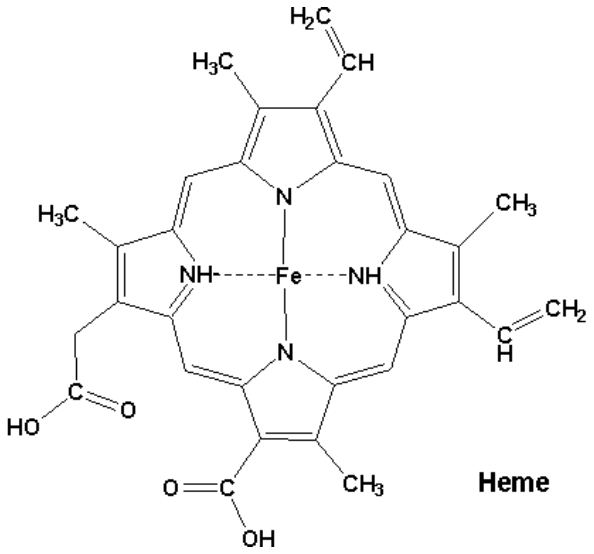

Figure 1.9 Structure of heme b cofactor in *M. tuberculosis* KatG

5-coordinated wild type KatG protein exhibits a Soret band at 407 nm additional absorption maxima at 505, 540, and 641 nm (Figure 1.10) (35). The 505 and 641 bands are due to the charge transfer in which electrons are transferred from the highest energy-

filled orbitals of the porphyrin to the lowest energy unfilled orbitals of the iron (40). Aside from the characteristic heme absorbance, KatG also shows a UV peak at 279 nm, which is due to the aromatic amino acid residues and additional contributions from the heme. The ratio of the absorbance at 407 nm to that at 279 nm is called the Reinheitzahl (RZ) value. This number has been used as an indictor of the purity of heme proteins. A general rule is that the higher number, the higher the purity. Freshly purified (5-coodinate) ferric KatG has an RZ value (this ratio is traditionally 280/407) around 0.56 in phosphate buffer. However, this value is affected by the iron coordinate number and by the buffer used to isolate the protein. For example, TEA-HCl buffer accelerates the conversion of 5-c heme to 6-c heme; for this reason, phosphate buffer is now used for isolation and purification.

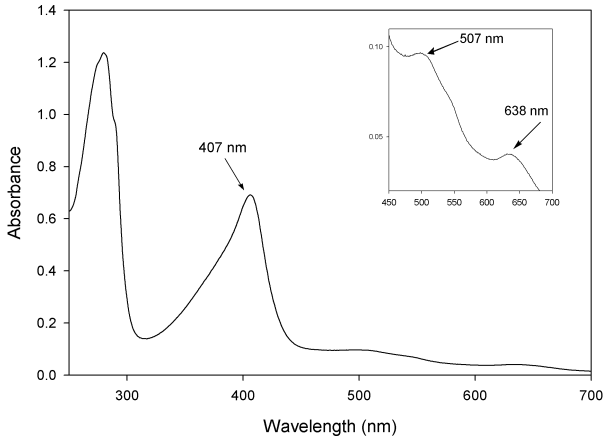

Figure 1.10 Optical spectrum of freshly prepared wild-type *M. tuberculosis* KatG. Inset shows the enlarged long wavelength region.

Like other heme peroxidases, resting *M. tuberculosis* KatG can be converted into several catalytic intermediates. Compound I formation and its characteristic optical

spectrum was reported by Chouchane et al. (35). This species, containing oxyferryl (Fe^{IV}=O) porphyrin π cation radical is formed in the presence of peroxyacetic acid. The molar absorption of Soret peak decreases by approximately 40% when resting enzyme is converted to Compound I, which is a typical feature of heme peroxidases. In addition, the Soret peak was found to shift to 411 nm. In the spectrum of KatG Compound I, two new maxima at 550 and 590 nm as well as a shoulder at 655 nm appear (Figure 1.11).

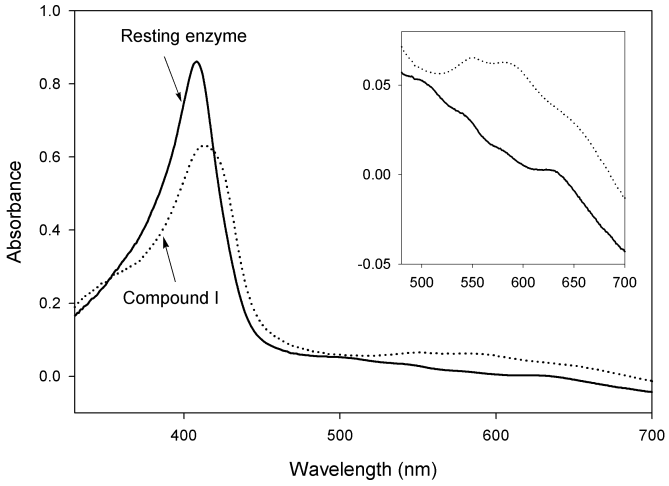

Figure 1.11 Optical spectrum of *M. tuberculosis* KatG Compound I. The Compound I intermediate of KatG was prepared by mixing resting KatG with peroxyacetic acid (10 fold).

Chouchane and colleagues detected another intermediate when KatG reacts with a large excess of hydrogen peroxide (~44,000 fold) (Figure 1.12). Its optical spectrum exhibits maxima at 418, 545 and 580 nm, resembling the bands of oxyferrous HRP (Compound III). Accordingly, this new species was assigned to KatG Compound III. A similar spectrum was also found in the reaction of KatG with superoxide (60).

The optical spectrum of Compound II has not been detected in WT *M. tuberculosis* KatG. An explanation of this fact is that Compound II of KatG is not stable and is quickly reduced to resting enzyme or converts to Compound III.

1.8 Techniques used to study peroxidase

During the last three decades, the research focusing on heme proteins has been facilitated by the introduction of overexpression and mutagenesis techniques. With milligrams of proteins being available to researchers, the formation of transient radicals can be monitored by rapid freeze-quench EPR spectroscopy, a technique that usually requires a large amount of sample. On the other hand, most of radical-forming proteins are colored due to the presence of their metallo-cofactors. Stopped-flow UV-vis and Raman spectroscopy techniques have been commonly employed to provide some important insights into their catalytic mechanisms. Protein crystallography and X-ray diffraction have been successfully used to solve the 3-dimentional structures of various peroxidases.

In our study of *M. tuberculosis* of KatG, these techniques have been frequently used and are very helpful in elucidating the enzyme catalytic mechanism and structural features. The important issues to which my thesis work was devoted include the characterization of aspects of the catalytic mechanism, including an assignment of a tyrosyl radical, and characterization of mutant enzymes, and a detailed analysis of mechanistic features of KatG catalytic function leading to formation of the acyl-NAD inhibitor molecule described above.

CHAPTER 2

IDENTIFICATION OF KATG TYROSYL RADICAL SITE

Protein-based radicals have been found by electron paramagnetic resonance (EPR) spectroscopy in a variety of enzymes. Inspired by the discovery that some protein radicals are involved in biological catalysis processes, the research in this field has attracted a lot of attention in the past two decades. Among the 20 natural amino acids, radical forming residues include glycine (61), cysteine (62), tyrosine (63), and tryptophan (64). All the amino acid based radicals are formed in posttranslational processes mediated by metal cofactors (65). The identification and characterization of those protein radicals has been very challenging, primarily due to their low concentration and transient stability.

When reacting with reactive oxygen species, such as peroxide and superoxide, many heme proteins form protein-based radicals. Aimed at finding similar process in *M. tuberculosis* KatG, Chouchane and colleagues mixed KatG with alkyl peroxide and successfully detected tyrosyl radical formation (66). However, the residue on which this radical forms required further study. The comprehensive characterization of this radical cannot be achieved without knowing its actual location in the protein. In this and the next chapter, we will discuss the work that we have done to elucidate the radical site in

KatG. Additional work addressing this issue involved mutagenesis of the residue identified by chemical analysis.

2.1 Introduction

Chouchane et al., demonstrated that *M. tuberculosis* KatG, like other peroxidases, forms Compound I when the resting enzyme (ferric) is treated with alkyl hydroperoxides (35). Furthermore, *M. tuberculosis* KatG Compound I can be reduced to the native state by a number of reducing agents including the antibiotic INH. However, the characteristic spectrum for Compound II was not detected in these experiments. It has also been shown that KatG Compound I decays quickly even in the absence of exogenous substrates, which indicates that an endogenous, amino acid based electron transfer pathway is likely present. This was also confirmed by Chouchane et al., in a recently published paper showing for the first time, a tyrosyl radical signal by rapid freeze quench EPR (RFQ-EPR) spectroscopy upon addition of peroxyacetic acid (PAA) to *M. tuberculosis* KatG (66). The yield of radical evaluated by quantitative EPR was near 0.2 spins per heme, which indicates that formation of this radical is not an artifact and that tyrosyl radical may play an important functional role in KatG enzymes. The initial rate of radical formation was unchanged using a 3-fold or 10-fold excess of peroxyacetic acid with respect to heme, suggesting that the radical is generated in a slow step following formation of an intermediate. Chouchane et al., proposed that tyrosyl radical is presumably formed through oxidation of the phenolic ring of tyrosine by Compound I formed from the resting enzyme and peroxide, in analogy to the reaction occurring in

prostaglandin H synthase (PGHS)(67,68). It is a very attractive hypothesis that this intermediate is KatG Compound I. However, neither its EPR signal nor its reduction to Compound II has been experimentally detected (66).

Tyrosyl radicals were also found in other heme and non-heme proteins such as myoglobin (69), photosystem II (70), bovine catalase(71), turnip peroxidase (72), Cytochrome c peroxidase (73) and Prostaglandin H Synthase (74). Tyr385 of PGHS, which is responsible for cyclooxygenase activity, is the only tyrosyl radical that is directly involved in a catalytic process.

Although the physiological substrate for KatG is not clear to us, some very interesting issues about this radical are worth pursuing: Why is tyrosyl radical so readily produced when KatG reacts with peroxides? Is the tyrosyl radical close to the heme center? Is this radical functioning like bovine liver catalase tyrosyl radical that protects the enzyme from forming non-functional intermediates (71)? And can it have a catalytic role separate from the peroxidase reactions catalyzed by heme iron? To answer those questions, the fundamental issue was addressed in this study: identifying the tyrosyl residue (or residues) capable of forming this radical.

2.2 Methods

The detection of radical forming sites in proteins is in general very difficult. In the study of KatG, EPR spectra alone could not predict the location of tyrosyl radical. The crystal structure of this protein had not been solved when this project was started. The difficulty also results from the fact that there are 21 tyrosine residues in each subunit

of *M. tuberculosis* KatG. The approach of site-directed mutagenesis involves a large workload, since there are a large number of candidates to be mutated. Furthermore, in the identification of the Tyr385 radical in PGHS, reaction of the Y385F mutant with peroxide produces a tyrosyl radical that is qualitatively similar by EPR spectroscopy to the radical produced in the wild-type enzyme (75). In our laboratory, a series of Tyr→Phe mutants were produced (Y113F, Y98F, Y155S, Y426F, Y304F) and examined by EPR spectroscopy. It was shown that all the mutants still exhibit tyrosyl radical formation. The inherent limitation of site-directed mutagenesis in combination with EPR spectroscopy for identifying the residue forming tyrosyl radical forced us to adopt a more direct approach.

Given the fact that the KatG tyrosyl radical is short-lived (decays in a few seconds), it is necessary to convert it to a stable species so that it can be identified more easily. Nitric oxide (NO) has been shown to react with the stable tyrosyl radical residue that is involved in the catalytic mechanism of ribonucleotide reductase, quenching the tyrosyl radical signal detected by electron paramagnetic resonance spectroscopy (76). Nitric oxide, a free radical, is expected to combine very rapidly with organic radicals such as the phenoxyl radical on a tyrosine residue. In another study, the reaction between tyrosyl radical and nitric oxide was fast enough to trap transient species (77). The inhibition of ribonucleotide reductase and the quenching of its tyrosyl radical EPR spectrum are reversible (78), suggesting that NO forms an intermediate that can decay back to the radical pair. This EPR silent intermediate is probably nitrosyl-tyrosine. Further oxidation of such an intermediate leads to the formation of 3-nitrotyrosine (79). In the case of PGHS, Goodwin et al. proposed that the peroxidase activity of PGHS

catalyzes the second step of oxidation (80). Below is a revised model (Figure 2.1) provided by Gunther et al. (79). Once nitrotyrosine is formed, the detection of nitrotyrosine containing peptide can be achieved by measuring its characteristic absorption at 365 nm (under acidic conditions).

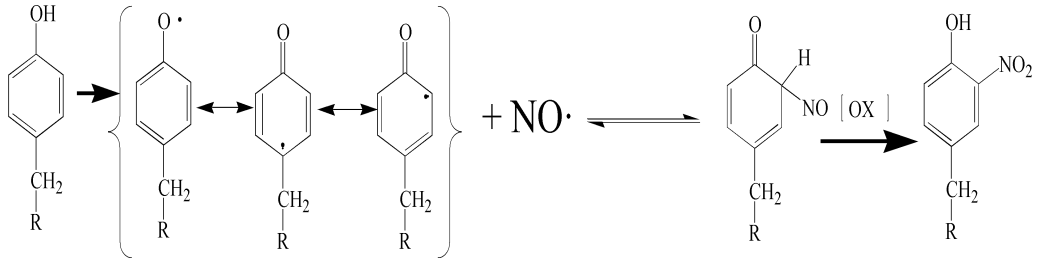

Figure 2.1 Proposed model of nitric oxide labeling of peroxidase tyrosyl radical.

In this thesis research, KatG tyrosyl radical was identified by using NO labeling in conjunction with peptide mapping techniques (Figure 2.2).

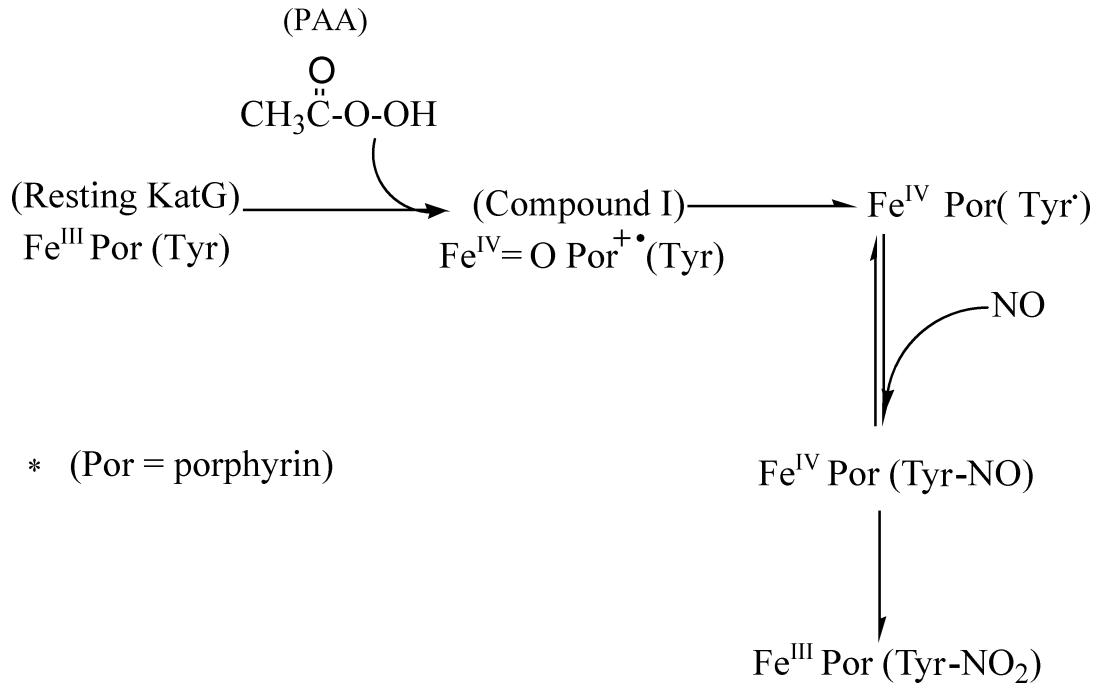

Figure 2.2 Formation of nitrated KatG by NO labeling of tyrosyl radical.

Nitric oxide was generated by controlled decomposition of an NO donor (for example, 1-[2-(Carboxylato) pyrrolidin-1-yl] diazen-1-ium-1,2 diolate). The donor used here is an unstable organic that releases NO from the [N(O)NO]- group as a function of change in pH, with a half-life (t½) of a few seconds at physiological pH (Figure 2.3). The amount of NO delivered can be roughly calculated by knowing the amount of donor that was added assuming complete decomposition of substrate.

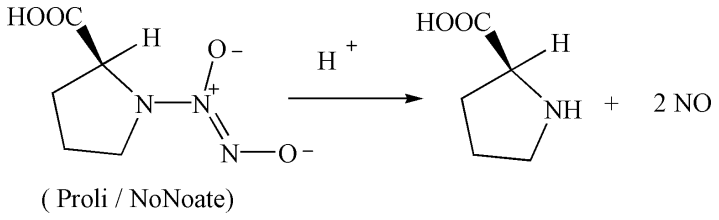

Figure 2.3 Release of nitric oxide from the donor Proli/NoNoate.

2.3 Results

2.3.1 Quenching of KatG tyrosyl radical by nitric oxide

The tyrosyl radical formed in KatG was first detected by Chouchane et al., using EPR spectroscopy. The same technique was also used here to first monitor whether the tyrosyl radical formed upon reaction of resting KatG with alkyl peroxides could be quenched by NO generated from a donor such as Proli/NoNoate (PROLI/NO). Figure 2.3 shows the results of an experiment in which a 3-fold excess of peroxyacetic acid was added to KatG in the presence and absence of the NO donor. Previous rapid freeze-quench EPR results demonstrated the formation of tyrosyl radical on a millisecond time scale under conditions similar to those used here, with the maximum yield of radical achieved after approximately 5 s (71). Here, the tyrosyl radical signal detected in the absence of NO (Figure. 2.4A) was completely quenched in the presence of NO. In the first protocol, peroxide was added to a mixture of the enzyme plus PROLI/NO that had been incubated for 2 s (Figure 2.4B). The two-sec time interval corresponds to approximately one half-life of the donor decomposition rate when it is exposed to neutral pH. Therefore, the concentration of NO in the mixture upon addition of peroxide was estimated to be equal to one equivalent per KatG subunit. The time interval during which enzyme was incubated with PAA was the same for both samples. Similar results were found when reversing the order of addition, such that the same total amount of PROLI/NO was added immediately after the addition of a three-fold excess of PAA to KatG (data not shown).

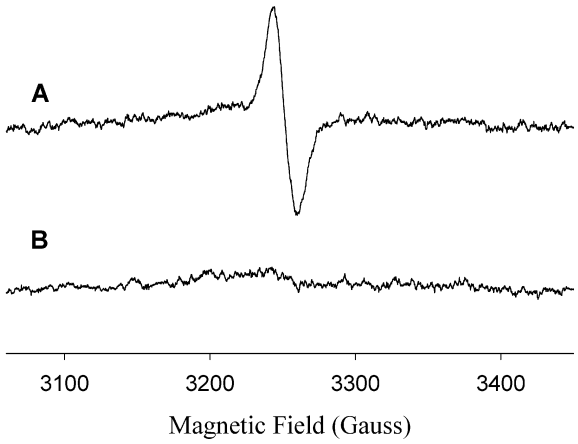

Figure 2.4 Quenching of tyrosyl radical in *M. tuberculosis* KatG by a nitric oxide donor. 50 µl of PAA (300 µM) were added to 50 µl KatG (100 µM, in 20mM phosphate buffer, pH 7.2) in the presence and absence of PROLI/NO and were immediately frozen by immersion of samples into liquid nitrogen. (A), absence of PROLI/NO; (B), KatG was premixed with PROLI/NO before addition of PAA. EPR conditions: microwave frequency, 9.23 GHz; microwave power, 5 mW; time constant, 1 s; temperature 77 K; modulation amplitude, 4.0 G.

2.3.2 Formation of nitrotyrosine detected by UV-Vis spectrometry

Having demonstrated the quenching of the tyrosyl radical EPR signal, we proceeded to seek evidence for nitrotyrosine in the treated enzyme. The HPLC profile of Proteinase K-digests of KatG treated with PROLI/NO and PAA showed several peptides with optical absorbance peaks both at 280 nm and 360 nm (Figure 2.5A). The absorbance at 360 nm provided clues that nitrotyrosine was present. The fragment eluting at 30 min., which had the highest absorbance at 360 nm, also exhibited an optical spectrum similar to that of authentic nitrotyrosine. Furthermore, when this sample was examined at pH 10, an absorbance maximum was found at 430 nm. The shift in absorbance maximum is expected upon deprotonation of the phenolic hydroxyl group of

nitrotyrosine (Figure 2.5B) (27). Similar results were obtained with the other major fractions having an optical absorbance peak at 360 nm (data not shown). These results are consistent with the presence of nitrotyrosine in multiple peptides. Since Proteinase K is a non-specific proteolytic enzyme, there is no specific information available from these HPLC profiles as multiple peptides could contain the same-labeled residue.

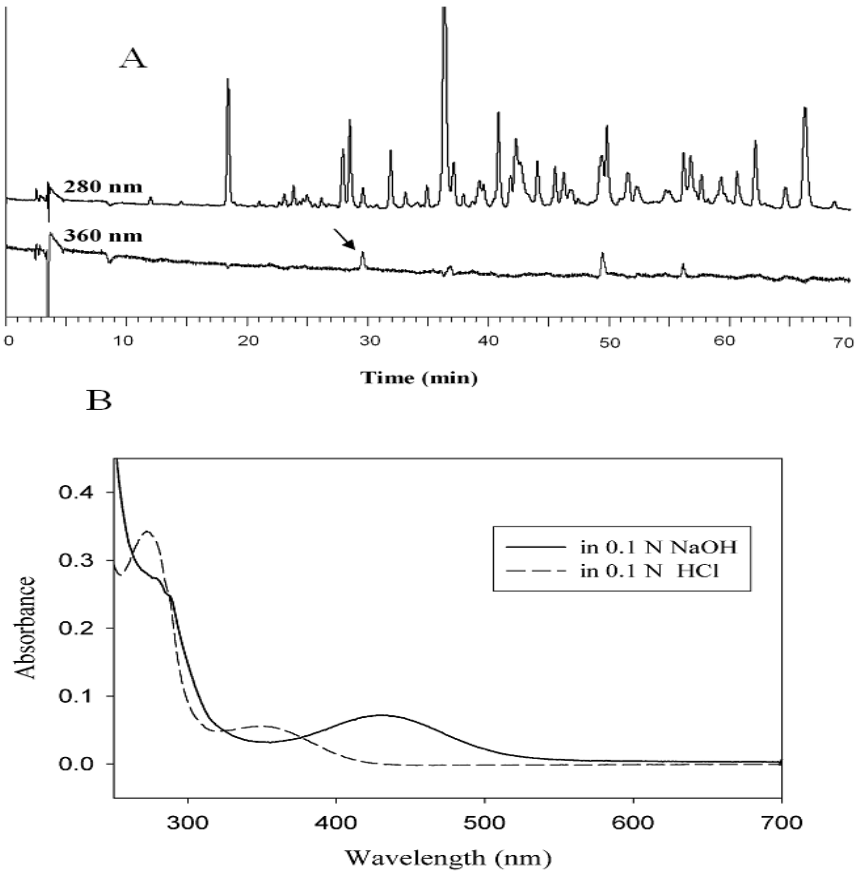

Figure 2.5 Identification of nitrated peptides derived from KatG. KatG was pre-treated with a 3-fold excess of PAA and one molar equivalent (relative to heme concentration) of PROLI/NO. (A), Reversed-phase HPLC profile (optical detection at 280 and 360 nm) of the Proteinase K digests of KatG. Nitrotyrosine has a characteristic absorbance at 360 nm at acidic pH; (B), UV-Visible absorbance of the peptide eluted around 29 min (indicated by the arrow in the HPLC profile), further purified, concentrated and re-dissolved in 0.1 N HCl or 0.1 N NaOH.

2.3.3 Specificity of nitric oxide labeling

In an effort to understand the specificity of the NO radical scavenging approach, and to rule out nitrotyrosine formation in KatG that could occur due to reactions that do not involve tyrosyl radical, a series of control experiments were carried out. In these experiments, a more specific protease, trypsin was used instead of non-specific Proteinase K. First, native or active enzyme was shown to be required for the formation of nitrotyrosine. For example, the protocol described above, in which NO-donor was added to KatG plus PAA, was repeated using KatG that had been denatured either by heating for 5 min at 100 ºC (Figure 2.6A), or by treatment with 6 M urea (data not shown). No nitrotyrosine was detected in the proteolytic digests of these samples. Likewise, tryptic digests from KatG reacted with PAA in the absence of NO donor, or with NO donor in the absence of PAA, did not contain nitrotyrosine (Figure 2.6 B and C). Nitrotyrosine was not observed in digests of KatG to which PROLI/NO was added 5 min after the addition of PAA, during which time tyrosyl radical will have completely decayed (66) (data not shown). These results demonstrate that nitrotyrosine is found only when catalytically active KatG, PAA and NO are present (Figure 2.6 D).

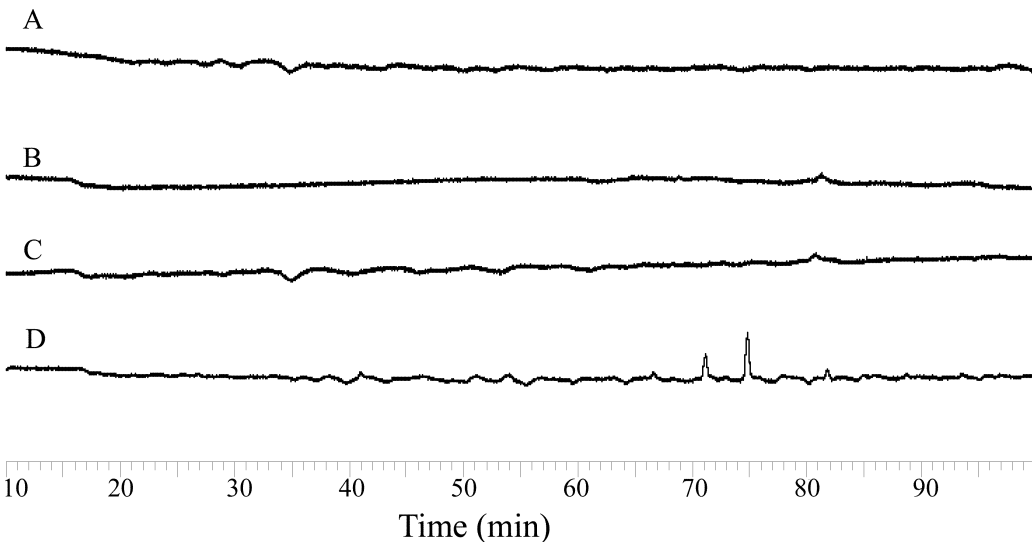

Figure 2.6 HPLC profile(A360 nm) of tryptic digests of KatG treated with PROLI/NO under various conditions. (A) KatG was denatured (at 100 °C for 5 min) before adding PAA and PROLI/NO; (B) KatG was treated with PAA only; (C) KatG was treated with PROLI/NO in the absence of PAA; (D) KatG was pre-incubated with PROLI/NO, PAA was added when half of the NO donor had decomposed**.**

To test the effect of the concentrations of nitric oxide and PAA on the yield of protein nitration, varying amounts (3, 6 and 10-fold excess) of PROLI/NO in combination with 3, 6 and 10-fold excess of PAA were used in a set of similar protocols. The labeling, tryptic digestion and HPLC separation were carried out as described above. The same two major nitrotyrosine-containing peaks (as in Figure 2.6 D) were consistently detected in all digests (data not shown for all samples). Although 3-fold excess of PAA was previously shown to be sufficient to generate a maximum yield of tyrosyl radical from resting KatG (9), in the labeling experiments, a maximum yield of nitrotyrosine was achieved using a 6-fold molar ratio of PAA and a 3-fold molar ratio of PROLI/NO (6-fold molar ratio of NO upon fully decomposing). Since the use of large excess of NO did not produce any new significantly nitrated peptides, these results strongly suggested that

a specific reaction, though possibly not at a unique tyrosine residue, was responsible for nitrotyrosine formation.

Using authentic 3-nitrotyrosine as an HPLC standard, we estimated that the maximum yield of nitrotyrosine was around 0.1-0.2 mol /mol KatG protein subunit. The estimated yield of tyrosyl radical by direct measurement using quantitative RFQ-EPR was around 0.19 spins/heme, which was considered low due to rapid decay of the radical. This yield of nitrotyrosine then reflects a highly efficient scavenging of tyrosyl radical and conversion of the proposed nitroso intermediate to nitrotyrosine.

2.3.4 Purification and sequencing of nitrated peptides

As shown in the HPLC chromatogram of Figure 2.7, the fractions eluting at 71 min and 75 min showed absorbance maxima at both 280 nm and 360 nm, which indicated peptides containing nitrotyrosine. These peptides were collected, concentrated, and subjected to further purification using a C8 reverse-phase HPLC column. The twice-purified peptides were subjected to sequencing analysis by automated Edman degradation. The results of a typical analysis are shown in Table 2-1: Peak 1 and Peak 2 refer to the HPLC fractions eluted at 71 min and 75 min respectively. Surprisingly, both nitrotyrosine-containing peptides had the same sequence, SPAGAWQYTAK. By comparison with the KatG amino acid sequence (Appendix 2), it can be seen that this fragment represents residues 346-356 of *M. tuberculosis* KatG.

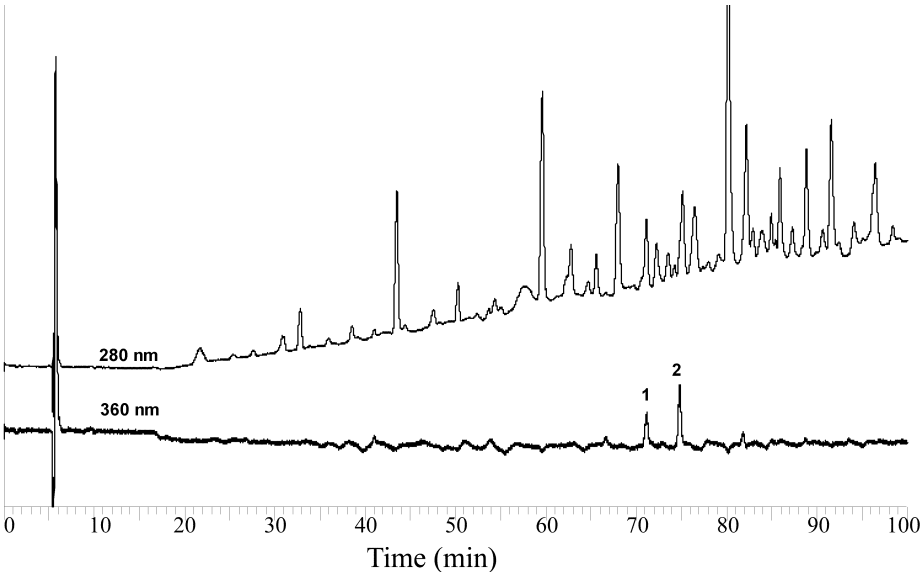

Figure 2.7 HPLC profile of tryptic digest of nitrated *M. tuberculosis* KatG. The sample was analyzed as described under Experimental Procedures using detection at 280 and 360 nm. The peaks (marked 1 and 2) at retention times around 71 and 75 min were further purified for sequence analysis.

The eighth cycle of the sequencing reactions for both peptides, which should indicate residue Y353, indicated a modified amino acid at this position. The phenylthiohydantoin (PTH) derivative of authentic 3-nitrotyrosine was prepared (as a service performed at the Laboratory for Macromolecular Analysis & Proteomics at the Albert Einstein College of Medicine) and run in a separate mock sequencing protocol. This species was found to elute at 15.17 min under the conditions used in the analysis of the KatG peptides. The modified KatG residue eluted at exactly the same time as the PTH derivative of 3-nitrotyrosine, which is evidence for the identification of this residue as nitrotyrosine. Furthermore, mass analysis using the MALDI technique showed that the $(MH)^+/z$ of the modified peptide (peak 1) was 1224, which is 45 mass units greater than the predicted mass of the unlabeled KatG tryptic peptide spanning residues 346-356. The

additional mass of 45 is exactly equal to that expected for nitration of a residue at which hydrogen is replaced by a nitro group (mass = 46). We note here that residue Trp 351 in the peptide represented by peak 2 was also modified, according to the sequencing profile of this fragment. The $(MH)^+/z$ of this fragment is 29 greater than that of peak 1, which could correspond to N-nitrosotryptophan (29). Assuming this is the product, the abundance of N-nitrosotryptophan was estimated based on a published extinction coefficient to be 30% of the total nitrotyrosine content (29).

Cycle	Peak 1	Peak 2
	Residue	Residue
1	S	S
2	P	P
3	A	A
4	G	G
5	A	A
6	W	?
7	Q	Q
8	Y^{nit} *	Y^{nit} *
9	T	T
10	A	A
11	K	K

* Y^{nit} : nitrotyrosine

Table 2-1 The Edman sequence analysis of nitrated peptides. Both nitrated peptides were isolated from the tryptic digest of niric oxide labeled KatG and were subsequently purified by HPLC before sequencing**.**

2.4 Discussion

Of the twenty-one tyrosine residues in *M. tuberculosis* KatG, nitrotyrosine was only found on residue 353. By close examination of the recently solved structure of *M. tuberculosis* KatG, we found that many tyrosine residues are solvent accessible. The reaction mixture used here did not generate an increasing yield of nitrotyrosine even when NO was provided in a significant molar excess. Since no change in the pattern of labeling occurred in the presence of increasing excesses of NO, we suggest that the unique labeling represents efficient tyrosyl radical scavenging by NO, and that reactions that could lead to non-specific nitrotyrosine generation are not producing detectable side products.

In previously published work (9), Chouchane et al. presented evidence that suggested formation of a unique tyrosyl radical in *M. tuberculosis* KatG upon turnover of the resting enzyme with alkyl peroxides even though two different EPR signals were detected. Here, our approach to the identification of the residue at which this radical is formed involved NO introduced under conditions known to generate the radical. A key feature of the success of this approach was the formation of nitrotyrosine, which allowed for confirmation of nitration in a single peptide at a unique tyrosine residue in KatG.

The mechanism for production of nitrotyrosine in KatG was not directly probed, but other reports provide a background and precedent for reaction pathways we suggest to be relevant here: It was reported that tyrosyl radicals in ribonucleotide reductase, photosystem II, and prostaglandin H-synthase enzymes reacted with NO (22,24,30). In the case of the heme enzymes PGHS-1 and PGHS-2, formation of nitrotyrosine was proposed to occur through heme-catalyzed peroxidation of the nitrosotyrosine initially

formed from NO and tyrosyl radical (23,24). Our results demonstrate the likelihood of a similar reaction pathway in *M. tuberculosis* KatG, which most likely involves:

1) Production of Compound I from the resting (ferric) enzyme and peroxyacetic acid, followed by;

2) Formation of a protein–based tyrosyl radical or radicals (including the possibility that tryptophan radicals are also formed) due to a spontaneous process defined in previous work on wild type and mutant KatG (9), followed by;

3) Quenching of this tyrosyl radical by NO released from the donor molecule, and

4) Heme-catalyzed oxidations ultimately producing a protein-based nitrotyrosine at residue Y353.

The secondary oxidation steps are possible due to the cyclic turnover of KatG peroxidase activity in the presence of the small excess of PAA used to initiate the first turnover in our experiments.

In the 3-dimensional structure, the phenol ring of Tyr-353 is found to be located about 14.6 Å away from the heme center and close to the surface of the enzyme. Most of the direct electron transfer found in many proteins has been reported to occur within the range of 10 Å. Thus, the relatively long distance between heme iron and Y353 suggests that radicals did not transfer directly from heme group to Y353. There might be another residue or residues involved in propagating the radical leading finally to the formation of Y353 radical. KatG enzymes have a conserved tryptophan (W321) residue located between the heme group and Y353 (Figure 2.8).

Figure 2.8 The positions of tyrosine and tryptophan residues in the N-terminal domain of *M. tuberculosis* KatG. This figure is modified from reference (44). The distances between residues are also shown (in Å).

W321 is about 5 Å and 9 Å away from heme and Y353, respectively. The homologous Trp (W191) in yeast Cytochrome c Peroxidase has been identified as the site of a stable tryptophanyl radical in that enzyme's Compound I (Compound ES) (81). There are no other redox active residues near W191 in yeast CcP, which may be accounted for highly stability of this radical species. The same Trp radical was also detected in ascorbate peroxidase (82). In HRP, the corresponding residue is a redox inactive phenylalanine, Phe221. However, when this residue was mutated to tryptophan (Phe221→Trp), a tryptophanyl was detected in the reaction of the mutant enzyme with hydrogen peroxide (83). Thus, W321 in KatG is highly likely to form a radical when KatG reacts with alkyl peroxide. Due to the presence of other redox active residues, the W321 radical can serve as part of the electron conduit chain from heme to Y353. If this hypothesis is true, a tryptophanyl radical would be theoretically detectable, yet this species was not seen in our study. The lower limit of sample freezing time using RFQ-EPR is 6.4 ms in these experiments. Therefore, any shorter-lived radical species could not be monitored. We have constructed a W321F mutant and characterization of the radicals formed in this mutant will shed some light on the radical processes observed in wild-type KatG.

Radical species are usually very reactive. Since the tyrosyl radical we have detected in KatG has a lifetime up to 10 seconds, it must be located in a relatively inert environment. The geometry of the phenolic ring and hydrogen bonding could also influence the redox potential of this group (33) and other factors may also be important for determining the stability of a protein based tyrosyl radical. In this case, its location at

the surface of the enzyme could explain why this residue is the final point of stabilization after electron transfers from the interior of the enzyme.

Our current results only confirmed nitrotyrosine formation at residue 353. Actually, there is another tyrosine residue (Y95), which is located about 8.8 Å away from W321 (Figure 2.7). It could also be a possible radical forming site.

Sequence alignment shows that Tyr 353 is unique to *M. tuberculosis* KatG. The residue at this position is conserved as a tryptophan in most other catalase-peroxidase enzymes. Whether or not radical formation at this residue is responsible for a special function of KatG in mycobacteria remains to be demonstrated.

We note here that modification of residue W351 in one of the nitrotyrosine-containing peptides is consistent with N-nitrosotryptophan formation. The modification of W351 in our experiments may or may not arise from reactions that involve a tryptophan radical since, for example, N-nitrosotryptophan is known to be produced using reagents such as N_2O_3, a nitrogen oxide that could be formed in the aerobic reaction mixtures of PROLI/NO donor used here (29). N-nitrosotryptophan would be expected to exhibit an optical absorbance at 360 nm (34). Since our HPLC results did not reveal a major contribution from peptides with absorbance at 360 nm other than those of peaks 1 and 2 (that is, there is specificity restricted to modification of residues W351 and Y353) we propose a second possibility: that a nitroso-tyrosine intermediate, initially formed from tyrosyl radical and NO at residue 353, functions as an NO-donor in close proximity to the indole nitrogen of the W351 residue and thereby facilitates its nitrosylation. These issues are worth clarifying in the future in order to understand electron transfer processes in KatG when is turns over in the absence of substrates.

CHAPTER 3

CHARACTERIZATION OF KATG[Y353F] MUTANT

The KatG tyrosyl radical was first investigated by Chouchane et al., primarily using EPR spectroscopy (66). In the previous chapter, we have demonstrated that Tyr 353 is a radical forming site that reacts with NO. In an attempt to have a better understanding of any catalytic roles of Y353 radical, a mutant protein was constructed by replacing the identified tyrosine residue (Y353) with a redox-inactive amino acid (Phe). Thus, the radical will not form on the Phe353 residue and any effects on the catalytic function of KatG can be tested. This chapter addresses the results of various analyses that have been performed on this mutant protein.

3.1 Construction and expression of Y353F mutant of KatG

The construction of the KatG[Y353F] mutant was carried out with a great deal of assistance from Dr Shengwei Yu. *E. coli* strain UM262 (84) carrying pKatII plasmid was used for over-expression of both wild-type and mutated KatG proteins. Mutagenesis was performed on pKatII using the QuickChange site-directed mutagenesis kit from Stratagene (La Jolla, CA). Pairs of complementary oligonucleotides were designed to introduce the required mutation indicated in boldface to produce KatG[Y353F] (A to T mutation, Tyr-Phe replacement, as shown below).

5’-1043CTGGCGCTTGGCAAT**T**CACCGCCAAGGACGG1073-3’

5’-1073CCGTCCTTGGCGGTG**A**ATTGCCAAGCGCCAG1043-3’

Mutagenesis was performed according to the manufacturer's protocol and the reaction products were transformed into super competent cells (*E. coli* XL1-Blue strain, Stratagene) for antibiotic selection and amplification. Sequencing (by Gene Wiz, Inc.) of the mutated *katG* gene confirmed that only the desired nucleotide substitution was present, and the mutated plasmid was then transformed back into *E. coli* strain UM262 for protein expression. During the purification process, the mutant protein behaved similar to the WT enzyme on various FPLC column media. The yield of mutant protein was comparable to that of wild type. Further, the mutant exhibited essentially identical optical spectrum features as wild type protein, having the same Soret peak wavelength maximum (407 nm) (Figure 3.1). These results indicate that the mutation did not bring about overall conformation change or significant modification at the heme-binding site. Like in wild-type KatG, the heme iron of freshly prepared Y353F mutant was a mixture of five coordinate and six coordinate, which is evidenced by the charge-transfer peak at 631 nm characteristic of 6-coordinate heme iron, and a shoulder at 380 nm only present in 5-coordinate heme.

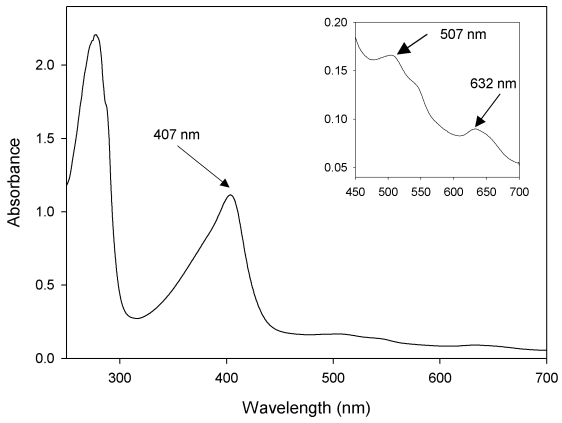

Figure 3.1 Optical spectrum of resting KatG[Y353F] mutant enzyme

3.2 Catalase and peroxidase activities of Y353F mutant

Y353F mutant enzyme showed exactly the same catalase activity as WT KatG (Table 3.1). As discussed in the previous chapter, both catalatic and peroxidatic cycles of KatG are initiated by peroxides and go through intermediate Compound I. The catalase reaction cycle also utilizes hydrogen peroxide as reducing substrate reacting with Compound I.

	WT KatG	[Y353F] mutant
Catalase	$(1.79 \pm 0.08) \times 10^3$ unit/mg	$(1.78 \pm 0.09) \times 10^3$ unit/mg
Peroxidase	1.06 ± 0.06 unit/mg	0.62 ± 0.03 unit/mg

Table 3-1 Catalase and peroxidase activities of wild-type KatG and Y353F mutant. The peroxidase activity was measured using *t*-butyl hydroxide and *o*-dianisidine. The catalase activity was measured by the decrease of absorbance of hydrogen peroxide at 240 nm. All the tests were repeated 5 times.

Hydrogen peroxide is a small molecule and can be easily fitted into the vicinity of heme site. Once compound I is generated by the first H_2O_2 molecule, the second hydrogen peroxide molecule can be directly oxidized by Compound I. Therefore, we speculate that due to the competition of H_2O_2 for Compound I, protein-based radical(s) will not be easily produced. This is consistent with the fact that no tyrosyl radical was

observed in WT KatG when reacting with H_2O_2 (66). As expected, the mutation of Y353 residue did not modify the catalase activity of KatG either.

On the other hand, the peroxidase activity of the mutant was found to be about 40% lower than wild type KatG (Table 3.1). In the peroxidase assay, a bulky peroxide species, *tert*-butyl hydroperoxide is routinely used as the oxidant and *o*-dianisidine (3,3'-dimethoxybenzidine hydrochloride) was the reducing substrate. The choice of *t*-butyl hydroperoxide as the standard assay substrate was made based on its aqueous solubility, and the low non-enzymatic rate of oxidation of reducing substrates (36), and the fact that is does not act as a reducing substrate of Compound I. Oxidation of *o*-dianisidine gives rise to a colored product that can be easily examined spectrophotometrically. Since wild-type and mutant enzymes exhibit exactly the same level of catalase activity, it is likely that Compound I, the only active intermediate of the catalatic cycle, was produced at the same rate for both enzymes. Therefore, it is likely that in the peroxidase cycle Compound I was also generated at equal rate for both enzymes. The second step of this cycle involves the oxidation of reducing substrates by Compound I. Compared with the wild type, KatG[Y353F] mutant showed reduced peroxidase activity. Considering that the mutation, being at the protein surface, is unlikely to alter the properties of the heme itself, and that Phe replacing Tyr on the surface is unlikely to alter access of *o*-dianisidine to the heme vicinity, we speculate that the reducing substrate used here could be, or at least in part, oxidized by Y353 radical in the wild-type enzyme. However, also possible is that the Phe is more hydrophobic than Tyr and there is some rearrangement of the enzyme surface that interferes with dianisiding getting where it needs to be to get oxidized.

It has been demonstrated that KatG can utilize some large sized molecules as substrates, such as NADH and NADPH. However, the heme group is deeply buried inside with a small channel (about 7 Å in diameter) open to solvent. An electron transfer pathway might exist, which conveys oxidation equivalents from the heme center to the enzyme surface. We speculate that Y353 residue might be at the ending point of such an electron transport chain. A similar phenomenon was observed in lignin peroxidase, in which a solvent accessible Trp residue (W171) is essential for the oxidation of veratryl alcohol (85,86). Mutagenetic substitution of Trp171 abolishes completely the veratryl alcohol oxidation activity of the enzyme. Chouchane et al. showed that the KatG tyrosyl radical can be quenched by INH. Therefore, it is a reasonable hypothesis that Y353 might play a similar role as W171 in lignin peroxidase. This idea can be tested in the future by comparing the peroxidase activities of wild type KatG with those of Y353F mutant using a collection of bulky reducing substrates.

3.3 KatG[Y353F] reaction with peroxides, an stopped-flow study

In order to characterize the mutant enzyme in preparation for EPR experiments to examine radical formation, optical stopped-flow experiments were carried out to examine the formation of catalytic intermediates in the Y353F mutant. Y353F mutant behaves like wild-type protein when mixed with small to large excesses of H_2O_2. No characteristic intermediates were observed spectroscopically when ferric Y353F (10 μM) was mixed with hydrogen peroxide (up to 5 mM). The proposed intermediate of catalase cycle, Compound I, was not observed either, probably due to its rapid reduction by H_2O_2.

Previous studies showed that wild-type KatG forms Compound I with alkyl peroxides, such as peroxyacetic acid. The product spectrum is characterized by a decreased Soret intensity (407 nm), including shoulders near 550 nm and 590 nm and a feature at 655 nm (35). Here, KatG[Y353F] mutant reacted with PAA and gave rise to an intermediate with a spectrum similar to wild-type KatG Compound I, however, the band features were not as clearly resolved as in wild-type enzyme. Figure 3.2 shows optical spectra of the intermediate formed in the mutant when reacting with PAA.

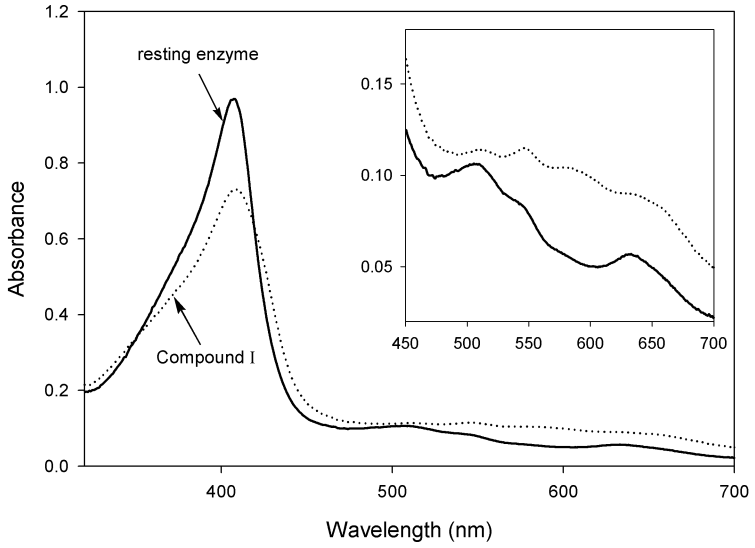

Figure 3.2 Optical spectrum of Compound I intermediate of KatG[Y353F].

Optical stopped-flow experiments using KatG[Y353F] revealed the formation of Compound I under the same conditions used to prepare the RFQ-EPR samples (3-fold excess PAA). This reaction was monitored at 590 nm, a typical peak for Compound I. As shown in Figure 3.3, during the first 30 seconds, both the WT and Y353F mutant showed

similar kinetics. The second-order rate constant for the formation of Compound I in KatG[Y353F] was determined from the rates observed in stopped-flow experiments performed as a function of peroxide concentration. The rate constant, on the order of 10^4 $M^{-1}s^{-1}$, is comparable with the second-order rates for the similar reactions in wild-type KatG (35). The rapid formation of Compound I was followed by a 10-second decay period, which we proposed, was caused in part by the formation of tyrosyl radical. The stopped-flow data agree well with the following freeze-quench EPR results, which showed that tyrosyl radical formation reaches its maximum yield in 10 s. There is still a little difference in the mode of Compound I decay: after compound I was formed in the Y353F mutant, there is a short period of plateau followed by a relatively rapid decay. While in the wild-type enzyme, the disappearance of Compound I was more steady (Figure 3.3).

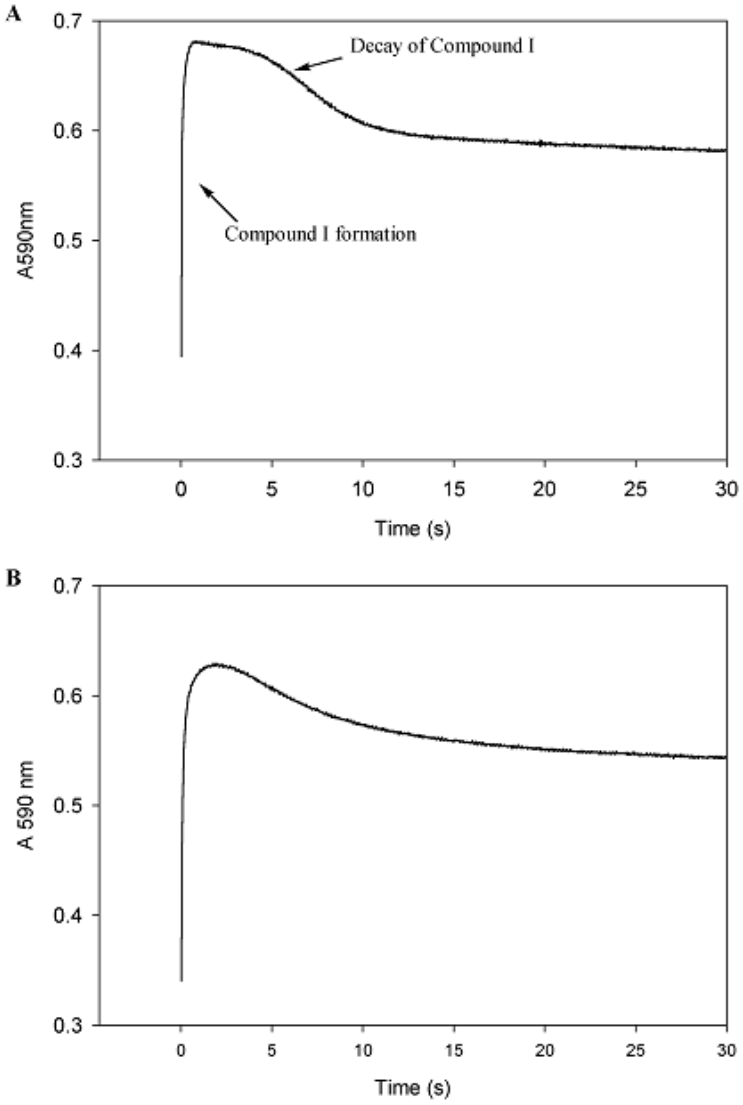

Figure 3.3 Formation and decay of KatG Compound I. The characteristic absorbance of Compound I at 590 nm was recorded for 30 sec using stopped-flow photospectrocopy immediately after KatG (wild type or mutant) was mixed with 3 fold PAA. A) Y353F mutant; B) Wild type KatG.

As reported for wild type KatG, no other intermediates accumulated during the interval following Compound I formation, though a single electron transfer producing tyrosyl radical would be expected to produce Compound II, which has a different optical signature from either Compound I or the resting enzyme. We suggest that in the mutant

as well as in wild-type enzyme, Compound II is unstable and cannot be detected. Also, the formation of Compound I at a rate similar to that of wild-type KatG allows for the rapid formation of tyrosyl radical in KatG[Y353F] as demonstrated in the RFQ-EPR experiments though the characteristics of this reaction and those of the tyrosyl radical are different in the mutant.

3.4 EPR study of radical formation in Y353F mutant

The most efficient way to study the radical species in an enzyme is through the use of EPR spectroscopy. In our previous EPR studies, mutations made on five tyrosine residues failed to provide significant changes in the tyrosyl radical formation in terms of kinetics and yields (except for Y229F, see below). Since we have successfully labeled the radical forming residue Tyr353, it was very important to carry out similar EPR studies on the Y353F mutant protein. By doing so, two issues will be addressed: 1) confirm the result from nitric oxide labeling; 2) observe if and how a new radical forms when the preferred tyrosine Y353 is missing. This part of the experimental work was carried out with the assistance of Dr. Stefania Girotto.

Rapid freeze quench EPR was used to monitor the reaction of Y353F mutant enzyme with PAA following the same procedure as previously reported with WT KatG (66). In these tests, the EPR spectra obtained at various time points showed that the Tyr→Phe mutation did not result in a complete loss of radical signal (Figure 3.4). Rather, similar radical spectra were observed. EPR line shapes, which are the doublet and singlet signals observed at various time points in this mutant, closely resemble those reported for WT-KatG (66) and are thus ascribed to tyrosyl radical or radicals.

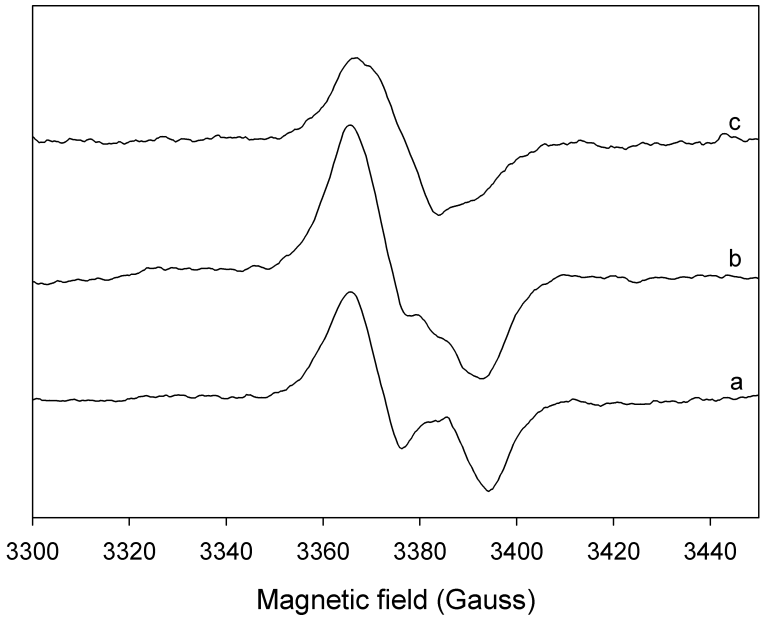

Figure 3.4 EPR spectroscopy of KatG[Y353F] mutant reacted with PAA. Rapid freeze-quench EPR samples were frozen 250 ms (a), 5 s (b) or 10 s (c) after mixing resting enzyme with PAA (final concentrations: KatG[Y353F], 50 μM; PAA, 150 μM) in 20 mM potassium phosphate buffer at 25 °C. EPR conditions: microwave frequency, 9.48 GHz; microwave power, 1.08 mW; time constant, 5.24 s; temperature 77 K; modulation amplitude, 1.0 G.

Even though tyrosyl radical was still formed, the yield of radical in the mutant was very low compared to that found for WT-KatG (Figure 3.5). The maximum yield of tyrosyl radical was calculated to be 0.05 spins/heme in Y353F mutant, which is about 73% less than that found in similar RFQ-EPR experiments on the wild-type enzyme. The amount of radical detected varied with the reaction time. The maximum yield of radical in Y353F mutant was observed at 100 ms, rather than the 10 s observed for wild type enzyme. Further, the evolution from the doublet to the singlet signal in Y353F mutant was slower than in the WT enzyme. These results demonstrate that a pathway to tyrosyl

radical formation still exists in the mutant enzyme, though oxidation of the new tyrosine residue occurs with significantly lower efficiency than in WT-KatG.

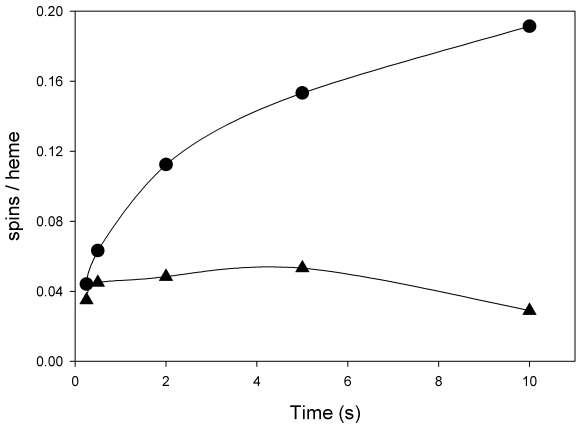

Figure 3.5 Time course of tyrosyl radical production in wild-type and Y353F mutant enzyme. RFQ-EPR samples were frozen after incubation for the indicated time intervals following the mixing of PAA with WT KatG (•) or KatG[Y353F] mutant (▲).

A small amount of peroxyl radical signal in the EPR spectra of WT KatG reacting with PAA was previously observed (87). The rapid freeze quench EPR spectra of Y353F mutant showed a relative larger contribution from the same signal, with g values g_z = 2.03, g_y = 2.006, g_x ~ 2.00. These observations suggest that the peroxyl radical observed in the RFQ-EPR spectra of the Y353F mutant enzyme is the result of a side reaction occurring with greater efficiency when the key tyrosine is unavailable. The significant increase of peroxyl radical yield in the RFQ-EPR spectra of the Y353F mutant confirms that the mutation of the tyrosine Tyr353 disrupts the native mechanism for tyrosyl radical formation. The identity of the peroxyl radical observed here was not determined. It could be an amino acid based peroxyl radical or a peroxide based peroxyl radical. Most

often, when a peroxyl radical is discovered in a heme protein treated with peroxide, it resides on a tryptophan; so, these results would be consistent with a peroxyl radical on a tryptophan when the final tyrosine is not available.

Taken together, the freeze quench EPR studies demonstrated that a tyroyl radical was still formed in Y353F mutant protein, but apparently on a residue different from that found in WT KatG. Further studies, such as those in which NO trapping was used, would help define the site of this tyrosyl radical. The interesting possibility that will be tested in the future is that a radical initially formed on W321 is easily transferred to tyrosines and ultimately is stabilized on residue Y353 but in the Y353F mutant, the electron transfer pathway to Y353 is interrupted allowing a radical on W321 to react with oxygen to give the observed peroxyl radical formed in very small yields in wild-type KatG.

3.5 INH activation by Y353F mutant enzyme

The activation of INH by KatG[Y353F] was measured by the inhibition of its target enzyme InhA. Compared with wild type KatG, Y353F mutant showed modestly reduced activity in the process. A detailed discussion regarding this experiment will be addressed in Chapter 4, section 4.2.

3.6 Discussion and conclusions

The mutation of Tyr353 residue would not be expected to induce major structural change either at the heme-binding site or in the overall protein. This was evidenced by

its behavior on various FPLC columns and its unchanged catalase activity. Thus, the only difference between the Y353F mutant and WT protein is a single residue replacement. Only under this condition can we deduce the role of Tyr353 in the catalytic pathway of WT enzyme by examining the Y353F mutant.

The reduced tyrosyl radical yield in the Y353F mutant was also associated with reduced peroxidase activity and slowed INH activation rate. It is possible that some reducing substrates can be oxidized by Y353 radical in the wild type protein. However, such conclusions must be drawn with great caution. The elucidation of an electron transfer pathway cannot be accomplished in a single mutation test. In the future, more work related to this pathway is needed.

The mutation of Y353 did not block tyrosyl radical formation on other residues, which is a very common phenomenon when using mutation techniques to study protein radicals. There are quite a lot of tyrosine and other redox-active residues present in this protein. The transfer of radicals from heme to other residues or from one residue to another is very common in metallo-proteins. We have also randomly constructed other tyrosine mutants. The mutants Y98F, Y113F, Y155F, Y304F and Y426F all behaved like wild type enzyme. Tyrosyl radical still formed in all these mutants. Thus, we eliminated the likelihood that any of these residues stabilize the tyrosyl radical we observed in the wild-type enzyme (66). It is worth noting that KatG[Y229F] mutant behaved very differently. However, an interesting fact about residue Y229 is that it is covalently incorporated into a three amino acid adduct located in a region near the distal side of the heme pocket (figure 3.6).

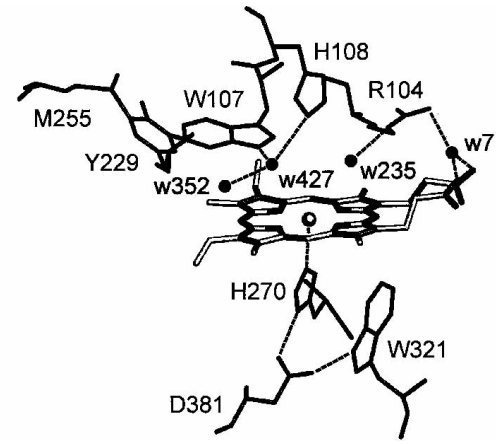

Figure 3.6 Y229 is involved in a three amino acid(Y229, M255, W107) adduct. This figure is adapted form Bertrand et al. (44).

The conversion of Tyr to Phe on this residue was found to have prevented formation of the adduct (88) in another KatG enzyme. Since those residues are located near the heme, the mutation would cause significant changes in the environment of the active site. We noticed that this mutant protein is more hydrophobic than is the WT KatG, which is evidenced by the longer retention time on a phenyl Sepharose column. This observation suggests that a significant conformation change may have occurred when Y229 was mutated. Additionally, the Y229F mutant totally lost catalase activity. In the earlier work on Y229F mutant in this laboratory, Yu et al., suggested that the observed tyrosyl radical was likely to be formed on the same residue as in wild-type KatG (50). Whether Y229 can also stabilize a radical under particular circumstances (yet not appear as nitrotyrosine in the NO trapping experiments described in Chapter 2) is currently under study since we believe that generation of the active site adduct involving residue 229, and methionine and tryptophan side chains, requires radical formation at one or more of these residues.

CHAPTER 4

HYDROGEN PEROXIDE INVOLVEMENT IN THE ACTIVATION OF INH BY *M. TUBERCULOSIS* KATG

4.1 Introduction

Isoniazid is a synthetic antituberculosis drug and has been used for over fifty years. However, the exact mechanism of its antibiotic effect has not been clearly elucidated. The growing appearance of INH resistant TB infections throughout the world has led to an increased interest in explaining the bactericidal function of this drug and the origins of drug resistance.

A major milestone in the research of the INH action mechanism was reached by genetic studies in 1992. Zhang and colleagues unambiguously demonstrated that *M. tuberculosis* KatG is required for INH sensitivity (27). INH is thus a pro-drug and is subject to oxidative reactions catalyzed by KatG. By simply mixing INH with KatG, Johnsson and Schultz detected several stable products including isonicotinic acid, isonicotinamide, and isonicotinaldehyde (4-pyridine carboxaldehyde) (56). However, none of these products showed significant bactericidal effects, a conclusion drawn years ago. The mechanism of INH activation by KatG has became clearer after a key cellular target was revealed as InhA, the fatty-acyl carrier protein-enoyl reductase. Johnsson et al. first demonstrated that InhA activity could be inhibited by the products of KatG

mediated reaction of INH with NADH. This process became more clear when an X-ray crystallography study showed that a covalent adduct isonicotinoyl-NAD (acyl-NAD) could be formed between INH and nicotinamide adenine dinucleotide and that this adduct could act as a competitive inhibitor for InhA enzymatic activity. (Figure 4.1) The adduct was first detected in a non-enzymatic O_2/Mn^{2+} catalytic system. Lei et al. later demonstrated that the same molecule could be produced through a KatG mediated process (59) but without a description of the mode of catalysis of the reaction.

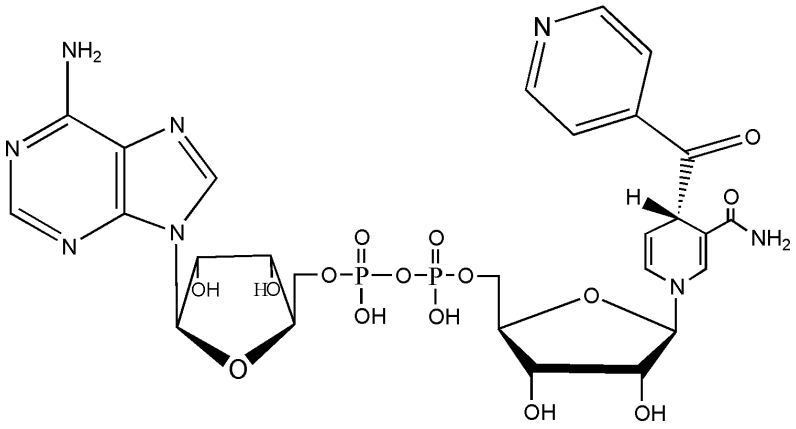

Figure 4.1 The INH-NAD adduct solved from crystal structure in which is bound to InhA (57).

Since KatG is assumed to function in INH activation as a peroxidase, the INH resistance due to the mutation in this enzyme should correlate to a loss of peroxidase activity. Actually, all the KatG defective (major deletion, or loss of heme) strains showed significant INH resistance. However, some exceptions do exist. KatG[S315T] mutant enzyme was found in more than 50% of INH resistant isolates. This protein exhibits only moderately reduced peroxidase activity when measured *in vitro* with typical peroxidase substrates (89). This may seem an apparent incongruity in explaining the

origin of relatively high drug resistance due to this mutation. However, this could be explained in that the standard peroxidase assays are utilizing various synthetic reducing substrates other than INH. Thus, the reaction between INH and KatG mutants cannot be estimated by simply looking at their peroxidase activity. For example, the specific interactions with INH are severely impaired (90,91) and a reduced affinity of INH for the mutant ferric enzyme was found for purified KatG[S315T], along with poor turnover of the drug by Compound I in this mutant (91,92).

Since the acyl-NAD could be the physiologically effective molecule in INH treated bacteria, the activation of INH by KatG has more recently come to be measured by production of this acyl-NAD adduct. This observation also leads to the expectation that KatG mutants from drug resistant *M. tuberculosis* strains would lack the ability to carry out generation of this molecule in similar reactions. In a study conducted by Wei et al., the authors showed that the ability of the KatG[L634F], KatG[A139P], and KatG[D735A] variants to activate isoniazid (measured as a function of the yield of the adduct) decreased by 36%, 76%, and 73%, respectively compared with wild-type enzyme. And the KatG[S315N] (another drug resistant mutant like S315T) and KatG[L619P] variants almost completely lost their abilities to convert isoniazid into the InhA inhibitor (93).

The reaction of INH with NAD(H) was first studied by Johnsson et al. This process is now believed to proceed with a radical species first formed on INH (56). In the presence of Mn^{2+} (90) or low concentration of H_2O_2 (93), a pronounced difference was observed between the wild-type and S315T mutant in their ability to reduce nitro blue tetrazolium (NBT), an assay used to measure free radical production in the presence

of INH. These observation are consistent with the proposal that the formation of INH-NAD adduct is initiated by an INH derived radical species, which can subsequently react with NAD^+ (94).

Then, an issue arises: how is INH oxidized into a radical species? KatG has been ascribed, in addition to catalase and non-specific peroxidase activity, a manganese peroxidase activity, NADH-oxidase activity, and hyrazinolysis activity. The INH oxidation by KatG intermediates has been previously investigated using optical-stopped-flow techniques in which Compound I was produced in reactions between the ferric enzyme and peroxyacetic acid or with m-chloroperoxybenzoic acid (35). The drug (INH) was found to be able to serve as a reducing substrate in a KatG "classical" peroxidase reaction, involving Compound I (35). Yu and colleagues further demonstrated that the rate of formation of Compound I from resting mutant (S315T) enzyme and those peroxides was very close to that for the wild type. Hence, the decreased rate at which the adduct was formed by the catalysis of mutant enzyme is stemming from a slow oxidation of INH by the Compound I intermediate of KatG[S315T] (92).

To date, several reports on the production of the acyl-NAD molecule/inhibitor using various approaches, many in the absence of KatG but with manganese as a redox catalyst, have focused on the structure of the product and its interactions with InhA, rather than on the specific catalytic function of KatG in its formation (58,90,94-96). The question raised here is, what peroxide species or other reactive oxygen species (ROS) are involved *in vivo* to convert resting KatG to its reactive intermediates and thus activate INH. If any ROS participated in this process *in vivo*, its effect of boosting inhibitor generation can be observed and modeled by an *in vitro* study.

Hydrogen peroxide is a very abundant ROS species in bacteria. And its possible role in the activation of INH has not been well characterized. In this report, we have chosen to adopt a biomimetic approach to evaluate the competence of KatG and KatG[S315T] mutant in producing InhA inhibition due to formation of the acyl-NAD adduct. Since we had previously shown that high concentrations of H_2O_2 are not useful for peroxidation of INH starting from ferric KatG (97), the generation of hydrogen peroxide in a continuous flow at very low concentrations is introduced as the novel methodology explored here. We suggest that Compound I provides a catalytically competent reactive intermediate for drug "activation" reaction paths, and show the poor catalytic function of the S315T mutant enzyme in producing InhA inhibition under these conditions. These experiments do not provide a detailed picture of all aspects of the drug activation mechanism but begin a systematic approach to explaining the function of KatG catalytic activity and take into account the relevant microenvironment in which this enzyme functions physiologically.

The issues addressed here include: 1) can ferric KatG initiate production of the previously characterized InhA acyl-NADH inhibitor in the absence of any exogenous peroxide or manganese?; 2) can the variables upon which the yield of this inhibitor depend be defined?; 3) can the origin of drug resistance in the mutant KatG[S315T] be understood based on the observations using a biomimetic reaction scheme?; 4) is there some dependence on the redox state of the nicotinamide dinucleotide cofactor used?

Additional issues raised in this report concern the role of the peroxidase-oxidase reaction arising in KatG in the presence of NADH.

4.2 Inactivation of InhA by INH catalyzed by KatG

KatG mediated InhA inhibition was first tested in the absence of exogenous peroxide. As shown in Figure 4.2, the inhibition of InhA (1 μM) was slow and reached about 86% after 1.5 hr of incubation, even though a relatively high concentration of wild-type KatG (0.5 μM) was used. This rate is comparable to those reported by Johnsson et al. (34,37). The KatG[S315T] mutant, found in the majority of INH resistant M. tuberculosis strains, was much less effective in catalyzing this process; only about 5% of the activity of InhA was lost after the same period of incubation. In the absence of KatG, the inhibition of InhA activity was negligible during the incubation.

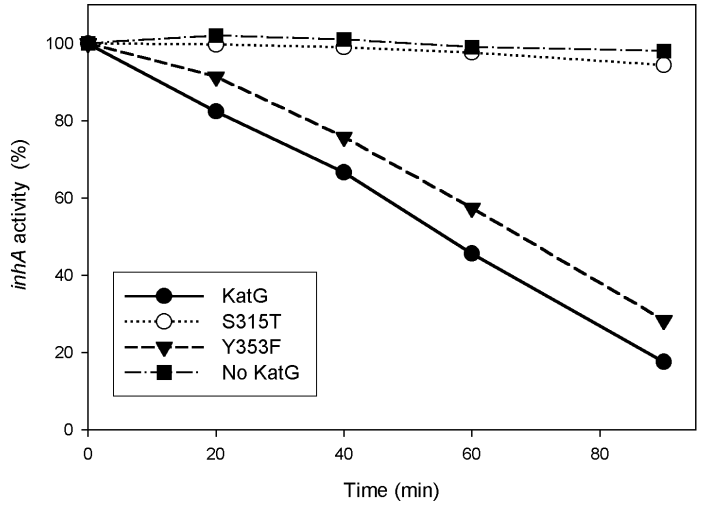

Figure 4.2 Inhibition of InhA activity by INH catalyzed by KatG or its variant. InhA (1 μM) was incubated with INH (50 μM), NADH (50 μM) and KatG (0.5 μM) or variants at 25°C. Aliquots were taken at indicated time points to measure InhA activity. Results are the mean of duplicate determinations with relative error less than 5%.

In a previous study, we proposed that a tyrosyl radical formed on tyrosine residue 353 when KatG reacts with organic peroxides might participate in drug activation. The Y353F mutant exhibits modestly lower (~60%) peroxidase activity and the same level of catalase activity, compared with wt. protein (98). When used to catalyze InhA inhibition, KatG[Y353F] mutant showed only a very small reduction in the rate of InhA inhibitor formation compared to wild-type KatG (Figure 4.2). This observation is good evidence that formation of the InhA inhibitor can proceed without participation of a radical on Tyr353. In Chapter 3, evidence for involvement of residue in *o*-dianisidine turnover was suggested, yet no function for this residue is found here. This could reflect differences in the rates of peroxidation on different substrates.

The adduct (inhibitor) formation in this simple mixture of INH, NADH, and KatG strongly suggested that some redox reactions were occurring to initiate catalysis. Furthermore, the inhibitor generated through catalysis by KatG has been reported to be the same species (acyl-NAD adduct) as one produced using only Mn^{2+} as a catalyst (59). The question then becomes, what is (are) the species responsible for initiation of a catalytically competent intermediate and what is this intermediate? Several routes exist through which a ferric peroxidase can be assigned a redox role in some pathway. Magliozzo and Marcinkevicene showed that the formation of a catalytically active enzyme from resting (ferric) *M. smegmatis* KatG in the absence of exogenous peroxide might occur as a result of iron reduction and binding of O_2 to give the oxyferrous form (Figure 1.7). However, re-crystallized INH in freshly prepared solutions does not reduce ferric KatG and only aged solutions of INH can accomplish such reduction. Thus, auto-oxidation of INH could induce catalytic turnover (97). On the other hand, the presence of

NADH and its known ability to be oxidized by oxygen in buffered solution, suggests that other autocatalytic processes such as the peroxidase-oxidase cycle described in plant peroxidases (see next section).

4.3 Effects of Catalase and *o*-dianisidine

Earlier literature in studies of the peroxidase-oxidase reactions showed that NADH in solutions could generate small amounts of H_2O_2 through the following reaction:

$$NADH + O_2 + H^+ \rightarrow NAD^+ + H_2O_2$$

This auto-oxidation process is faster in acidic solution than in neutral environment. The released H_2O_2 even at very low levels can initiate the peroxidase cycle and then catalytic NADH oxidation in HRP (53,99). To investigate whether endogenous H_2O_2 was also generated in our INH, NADH, enzyme reaction mixtures, and to test its possible impact on the reactions leading to inhibition of InhA, varying amounts of bovine liver catalase were included in our INH activation experiments. As shown in Figure 4.3A, in the presence of 0.25 μM bovine liver catalase (BLC), the rate of inhibition of InhA was much slower than without catalase and the reduction in rate was greater using higher concentration of catalase (0.5 μM). It should be mentioned that KatG also exhibits robust catalase activity with a Km for H_2O_2 in the order of mM, which is around 10 fold less than that of BLC (34). Therefore, these observations suggest that the abundance of catalase activity in the mixtures containing added BLC scavenges enough endogenous H_2O_2 to limit a peroxidative pathway to the InhA inhibitor. The catalase

cycle of KatG can be interrupted after Compound I formation if hydrogen peroxide production is slow enough that the second turnover with another molecule of H_2O_2 is negligible or under conditions at which the concentration of peroxide is always well below Km for the binding of a second peroxide molecule to Compound I. The observation that KatG[Y229F] mutant, which lost its catalase activity, can still form Compound I and also has *o*-dianisidine peroxidase activity, and can catalyze the formation of the INH-NAD adduct (data not shown) illustrates that once Compound I is available, peroxidation can occur under conditions where catalase turnover does not. Added together, these facts suggest that BLC competes with KatG (0.5 μM) for the limited H_2O_2 produced in situ and thereby reduces the catalytic turnover of KatG and the yield of inhibitor. To further explore the mechanism of these reactions, a bona fide peroxidase substrate was tested for its ability to interfere with inhibitor production.

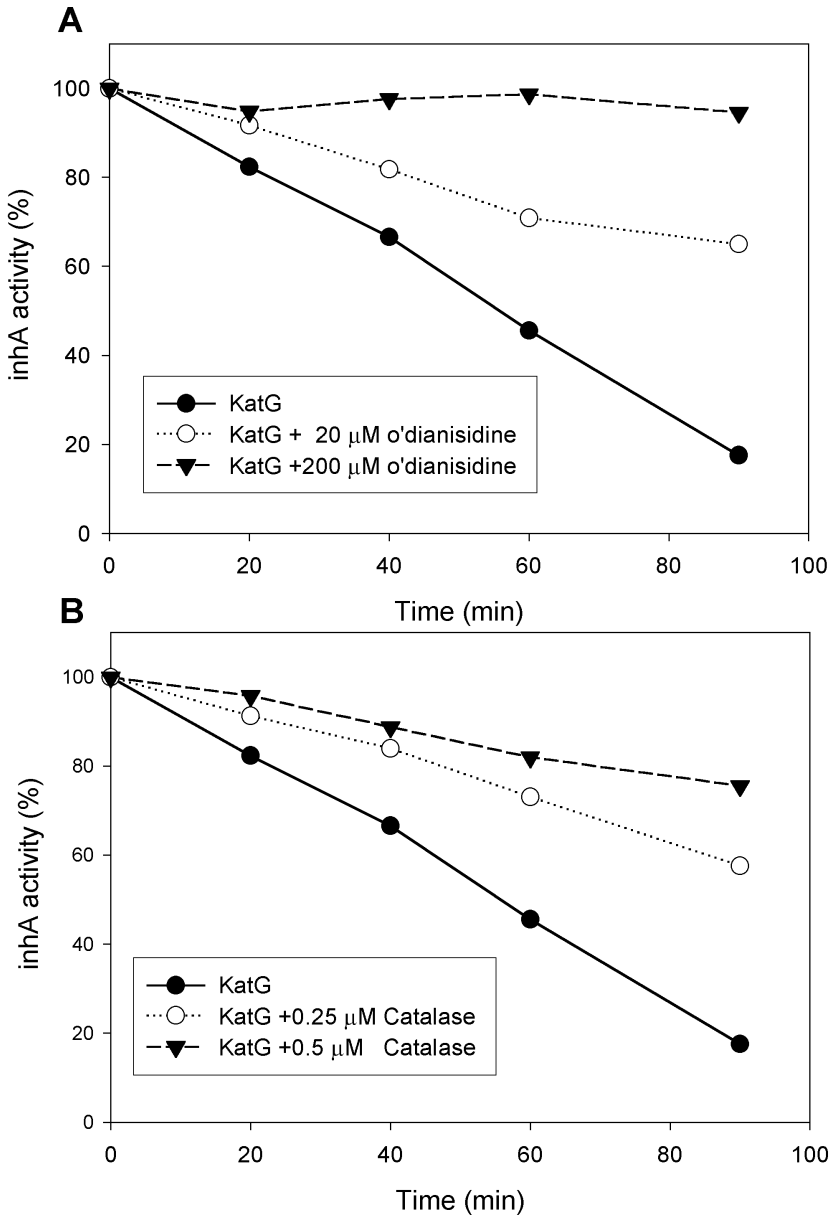

Figure 4.3 Inhibition of InhA activity by INH catalyzed by KatG in the presence of *o*-dianisidine or catalase. InhA (1 μM) was incubated with INH (50 μM), NADH (50 μM), and KatG (0.5 μM) at 25°C. Aliquots were taken at indicated time points to measure InhA activity. Results are the mean of duplicate determinations with relative error less than 5%. (A) *o*-dianisidine (20 or 200 μM) was included in the reaction mixture. (B) Bovine liver catalase (0.25 or 0.5 μM) was added to the reaction mixture.

Dianisidine is a widely used substrate for peroxidase catalytic activity assays and is a substrate for Compound I and II in a peroxidase cycle. Its ability to inhibit INH-NAD production via the KatG peroxidase cycle was investigated here. In our study, when 20 μM *o*-dianisidine was added to the mixture of INH, NADH and KatG, the generation of InhA inhibitor was much slower than without dianisidine (Figure 4.3B). In the presence of 200 μM o-dianisidine, the inhibition of InhA was nearly completely absent after 90 min of incubation, suggesting that the production of the INH-NADH adduct was effectively blocked. These results are considered strong evidence for the peroxidase cycle of KatG, initiated by endogenous hydrogen peroxide formed in the presence of NADH, being responsible for catalyzing production of the inhibitor of InhA.

4.4 Effect of slow generation of H_2O_2 by glucose/glucose oxidase

If H_2O_2 plays a role in the generation of INH-NAD adduct mediated by KatG, the addition of exogenous H_2O_2 should boost the yield of the inhibitor. Separate experiments (data not shown) had demonstrated that addition of a bolus of H_2O_2 to reaction mixtures such as those described above produced very poor to undetectable yields of InhA inhibitor and in earlier work it was also shown that a bolus of H_2O_2 did not enable efficient INH oxidation by KatG (60). Here, a simulated in vivo oxidative environment was tested such that H_2O_2 was generated in the reaction mixture at a continuous very low level by the addition of glucose and glucose oxidase, which catalyzes the following reaction:

$$Glu + O_2 \leftrightarrow gluconolactone + H_2O_2$$

In the presence of 2 mU/ml or 10 mU/ml GOx, the rates of H_2O_2 production were separately shown to be 0.4 μM/min and 2.0 μM/min, respectively. As shown in Figure 4.4A, the H_2O_2 enzymatically generated in situ accelerated the inhibition of InhA such that 2 μM /min H_2O_2 increased the inhibition by a factor of 2.5 within 90 min, and was more efficient than 0.4 μM /min H_2O_2. When INH is omitted from the mixture, no detectable inhibition was found after 90 min of incubation, ruling out inhibition of InhA due to undefined reactions taking place in the presence of G/GOx and the other reagents. Similar results were observed by multiple injections of authentic H_2O_2 (approximately one-half equivalent per injection over one hour) using an automatic titration apparatus (data not shown). These observations demonstrate that a constant low level of H_2O_2 enhanced the KatG mediated generation of InhA inhibitor. In *E. coli*, the concentration of intracellular H_2O_2 is controlled at the 10^{-7} M level by the regulation of several enzymes (100). Even though we do not know the exact concentration of H_2O_2 in the *M. tuberculosis* cell, the maximum amount of H_2O_2 employed here (2.0 μM/min) would be physiologically relevant. Therefore, we speculate that similar reactions could also occur *in vivo*.

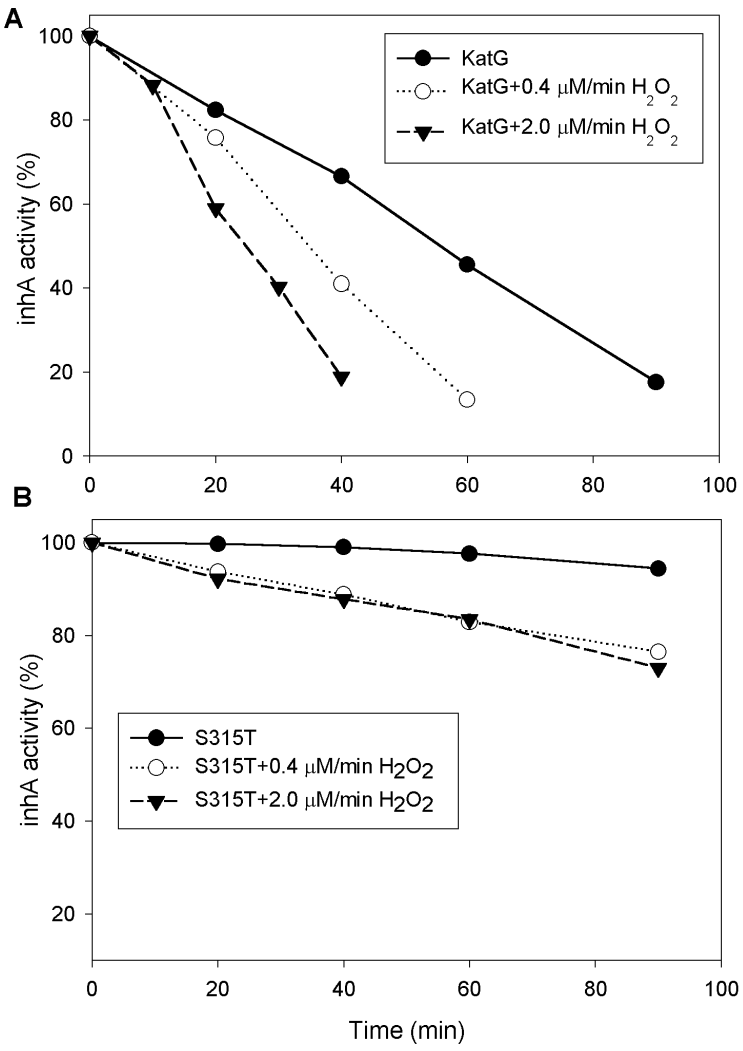

Figure 4.4 Inhibition of InhA activity by INH catalyzed by KatG or S315T in the presence of H_2O_2. InhA (1 μM) was incubated with INH (50 μM), NADH (50 μM), and KatG (0.5 μM) at 25°C. H_2O_2 was generated in the reaction mixture through glucose/glucose oxidase system. Results are the mean of duplicate determinations with relative error less than 5%. (A) by KatG; (B) by S315T mutant.

Similar experiments in which the INH resistant mutant KatG [S315T] was used in place of wild-type KatG also showed modest increases of InhA inhibition in the presence of G/GOx (Figure 4.4B). However, a lower extent of inhibition during similar periods was found (for example, 40% residual InhA activity vs. 90% remained after 30 min for

wild-type KatG and the mutant, respectively). This result is evidence that the reactions leading to the inhibitor are KatG-dependent and do not arise due to reactions from other redox pathways that occur in the presence of G/GOx. In reactions using KatG[S315T], the extent or rate of inhibition of InhA using 2.0 μM/min H_2O_2 was comparable to that using 0.4 μM/min, which may indicate a rate limiting step that is peroxide independent, in contrast to the results with wild-type KatG. This apparent "saturation" in the production of an intermediate at both low and higher concentrations of peroxide suggests that the rate limiting species is the S315T-INH complex and even if more resting KatG gets turned over to Compound I with more peroxide production, the same fraction of KatG molecules have INH bound and susceptible to peroxidation: therefore, the rate will NOT be dependent on peroxide (and Compound I concentration) but on INH concentration. This is consistent with previous stopped-flow measurements showing that the rate of reduction of Compound I in wild-type KatG and KatG[S315T] in fact depends on INH concentration (92). The observation of inhibitor formation catalyzed by the mutant is consistent with reports that *M. tuberculosis* strains bearing the S315T mutation in KatG are still susceptible to INH but with MIC's that can be as high as 200 fold higher than that for wild-type strains (33,101,102).

H_2O_2 is a major physiological reactive oxygen species. Previous studies showed that adding exogenous H_2O_2 induces the expression of KatG in *E. coli* and *M. tuberculosis* cultures (103-106). As the only catalase in *M. tuberculosis*, KatG is the principal H_2O_2 scavenger that responds quickly to destroy H_2O_2. Upon infection, *M. tuberculosis* is engulfed by macrophages in the lungs (107,108). Hydrogen peroxide along with other molecules plays a role in the host immune response to the intracellular

pathogens. Recently, a KatG knock-out strain of *M. tuberculosis* was produced and the role of the catalase activity of the enzyme was clearly shown to be required for virulence (109). Another study showed that hydrogen peroxide also promoted the INH susceptibilities of susceptible and resistant (KatG mutant) M. smegmatis strains (110). The reasonable question then arises, could hydrogen peroxide potentiate INH activation (peroxidation) in vivo even though KatG is an efficient catalase? This is theoretically feasible because both the catalatic and the peroxidatic cycles in KatG share the kinetically competent intermediate, Compound I. A very low level of hydrogen peroxide would be expected to limit the rate of catalase turnover and still support Compound I formation (if the reaction cycle occurs in two steps), which can then be diverted in the presence of an oxidizable substrate such as INH.

4.5 InhA inhibition using NAD^+ *vs.* NADH

NADH and NAD^+ have both been used for the in vitro generation of InhA inhibitor in other studies (37,95,96). However, the difference in behavior between these two species has not been carefully examined, nor has a specific effect been defined. In this study, we found that in the absence of added H_2O_2, NADH is much more efficient (2-3 fold faster) than NAD^+ in reaction mixtures producing inhibition of InhA (Figure 4.5). This observation is consistent with some previous in vitro studies (34,55,56,58). However, when H_2O_2 (2 μM/min, generated through G/GOx) was included with NAD^+, InhA activity was totally inhibited in 8 min, compared with 50 min starting with NADH in the reaction mixture (Figure 4.5).

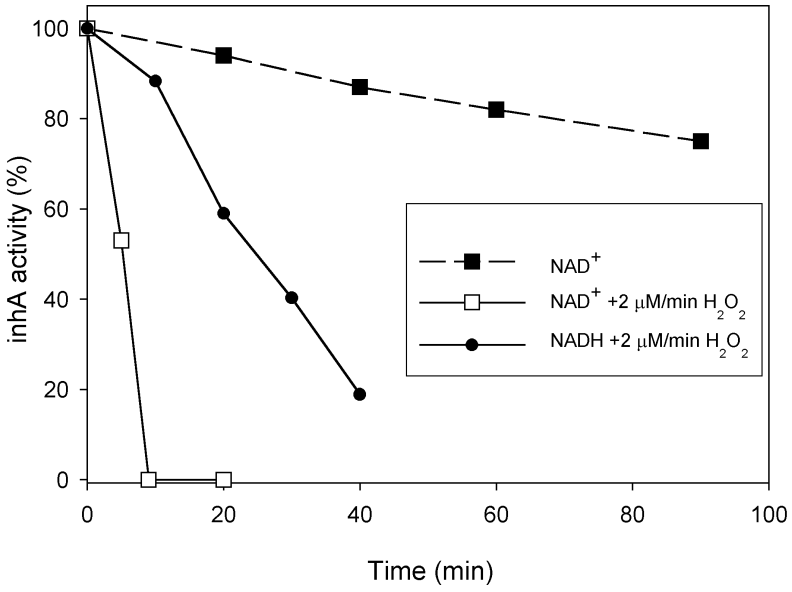

Figure 4.5 Effect of H_2O_2 on inhibition of InhA by INH and NAD^+. InhA (1 μM) was incubated with INH (50 μM), NAD^+ (50 μM), and KatG (0.5 μM) at 25°C in the presence or absence of exogenous H_2O_2. H_2O_2 was generated through glucose/glucose oxidase system. Results are the mean of duplicate determinations with relative error less than 5%. For comparison, the result using NADH (50 μM) instead of NAD^+ under same conditions is also included.

Several group proposed that NAD^+, rather than NADH, is the reactive form of the cofactor that reacts with INH. Then, why was NADH more effective in the generation of inhibitor than NAD^+ in the absence of exogenous H_2O_2? This was due to, as we proposed, the oxidation of NADH in aerobic solution, which produces a small amount of H_2O_2. This trace amount then turns on the peroxidatic cycle of KatG and thus stimulates the yield of InhA inhibitor. When enough exogenous peroxides (such as H_2O_2 used here) are supplied, NADH will act as a reducing substrate of KatG Compound I and compete with INH. In the case, NAD^+ is more efficient.

It is worth noting that inhibitor (adduct) was slowly produced starting with NAD^+ could arise due to slow auto-oxidation of INH, which has been shown to be able to initiate the catalysis of KatG (97).

These results are consistent with NAD^+ being the reactive form of the cofactor. This observation also supports our hypothesis that NADH serves as a source of H_2O_2 when mixed with ferric *M. tuberculosis* KatG.

Several genetic studies reported significant INH resistance in some NADH dehydrogenase defective M. smegmatis stains, which also exhibited raised the cellular $NADH/NAD^+$ ratio(111,112). Those observations may be interpreted in light of the findings here. The drug resistance from those mutants can stem from two things:

1) Higher concentration of NADH will compete with INH for the Compound I of KatG, since both of them are reducing substrates for Compound I. As a result, the INH-NAD cannot be generated effectively when NADH levels are high. This is evidenced in our above-described in vitro test in which NADH is less efficient than its oxidized form in producing adduct/inhibitor.

2) Since NAD^+ is the reactive form interacting with a species derived from INH peroxidation, its lower cellular concentration will reduce its availability for generating adduct/inhibitor, especially when other physiological processes also compete for this cofactor species.

4.6 Spectroscopic confirmation of InhA inhibitor

To confirm that the remarkably enhanced inhibition of InhA in the presence of G/GOx is due to the fast formation of the previously characterized INH-NAD adduct, and that the production of this adduct is independent of InhA, a reaction mixture was prepared containing INH, NAD^+, KatG and G/GOx in the absence of InhA. After a brief incubation of this mixture and subsequently removal of KatG and GOx, InhA was added to trap the generated inhibitor**.** The INH-NAD adduct is a very tight-binding inhibitor with an overall inhibition constant (Ki) of a few nM (58). After extensive gel filtration, NAD^+ and other reagents were removed and the inhibitor remained bound to InhA evidenced by the shoulder at 320nm in the optical spectrum of the recovered InhA. This absorbance is due to tightly bound INH-NAD adduct, and reproduces results in other studies (59). When G/GOx was omitted, the shoulder was not detected, which also confirmed that in the absence of peroxide, the formation of adduct/inhibitor is a very slow process (Figure 4.6). These observations demonstrated that the G/GOx induced inhibition of InhA occurs through the production of the INH-NAD adduct rather than some modification of InhA occurring in the reaction mixtures described in the previous experiments.

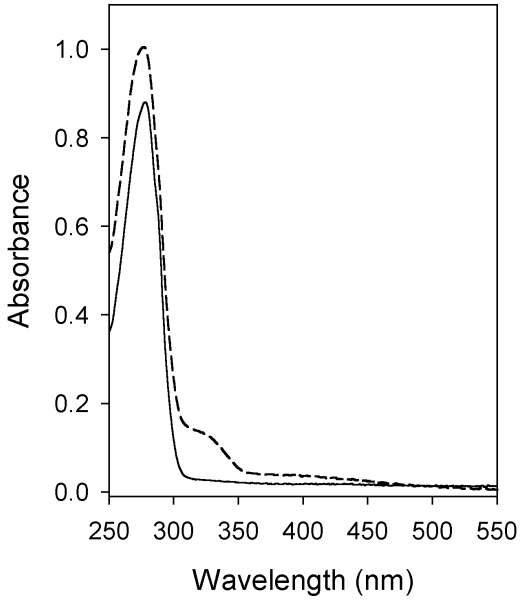

Figure 4.6 Optical spectra of inhibitor bound InhA complex. The INH-NAD adduct was first generated in a reaction containing INH (200 μM), NAD^+ (200 μM), KatG (1 μM) in the presence (dashed line) or absence (solid line) of H_2O_2 (generated by G/GOx). The INH-NAD adduct was harvested by allowing it to bind to InhA and the inhibitor bound InhA complex was purified according to the method section. The shoulder at 320 nm shows the presence of InhA bound adduct/inhibitor.

4.7 INH concentration dependence

The free INH-NAD adduct has a characteristic absorbance at 326 nm, a wavelength at which NAD^+, INH and its oxidation products showed no significant absorbance. Therefore, the generation of INH-NAD can be monitored spectrophotometrically in reaction mixtures containing KatG, drug and cofactor. When any of the three reactants (KatG, INH, and NAD^+) was omitted, there was no detectable absorbance increase at 326 nm (in the presence of G/GOx). As shown in Figure 4.7, when the amount of NAD^+ is fixed at 50 μM, the yield of INH-NAD adduct was

dependent on INH concentration. These results are consistent with a reaction path that depends on the rate of drug turnover into a reactive intermediate. Interestingly, the KatG mutant enzyme S315T required millimolar concentrations of INH to produce the INH-NAD adduct at rates approaching those observed for the wild-type enzyme using micromolar drug. The difference in the rates of inhibitor generation observed using these two KatG enzymes is coincident with the up to 200 fold difference in MIC between wild type *M. tuberculosis* and its S315T mutant strains treated with INH in vitro (33,101,102). This result is quite important since the only difference between the two sets of results is the concentration of INH. The concentration of Compound I in the system is expected to be close to the same for wild type and mutant. Since the mutant enzyme has catalase and peroxidase activities (with *o*-dianisidine) close to those of the wild type enzyme, the drug resistance mechanism is associated with the poor reaction of the mutant specifically with INH. Also, previous work demonstrated a 160-fold reduction in affinity of KatG[S315T] for INH compared to wild-type enzyme and a reduced reaction rate between INH and Compound I of the mutant (92).

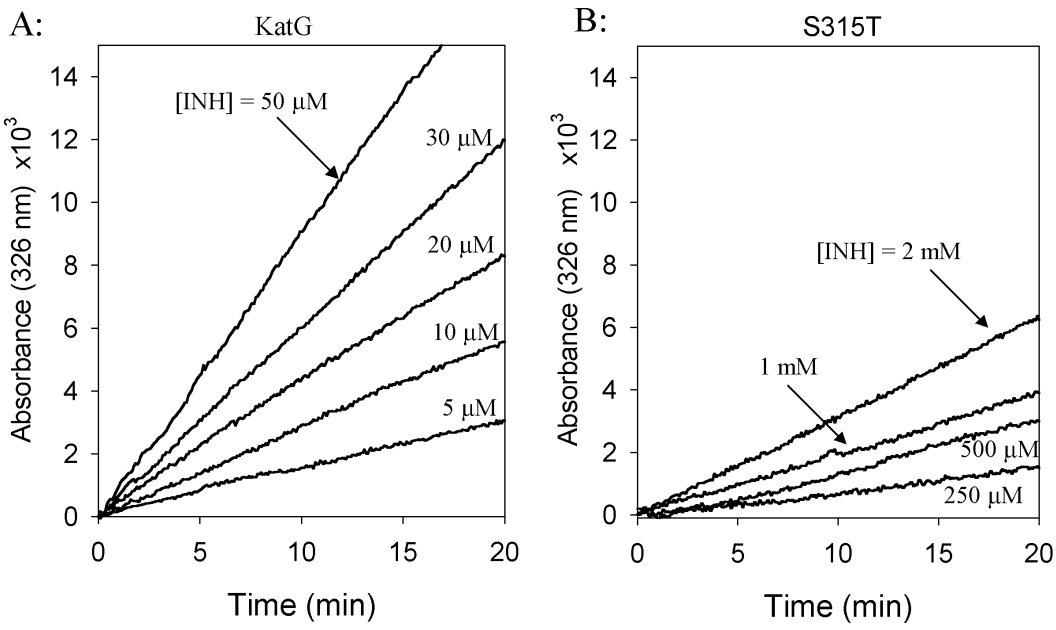

Figure 4.7 Effect of INH concentration on the production of INH-NAD adduct. The INH-NAD adduct formation was monitored by its characteristic absorbance at 326 nm. KatG (0.5 μM), NAD^+(50 μM), and H_2O_2 (2 μM/min, generated enzymatically) were incubated with varying amounts of INH. A: 5, 10, 20, 30, and 50 μM INH catalyzed by KatG; B: 0.25, 0.5, 1, and 2 mM INH catalyzed by S315T mutant.

In the context of drug resistance mechanism, our results also help explain the origin of INH resistance in strains bearing the S315T mutation in *M. tuberculosis* KatG. In this mutant, the yield of inhibitor can be raised up to physiologically relevant amounts simply by supplying higher concentrations of INH. This is completely consistent with known features of the structure of this mutant in that the replacement of threonine for serine interferes with INH binding productive for drug oxidation yet does not interfere with catalytic function of the heme itself.

4.8 Discussion and Conclusions

Since the structure of INH-NAD adduct was described by Rozswarski et al., many studies related to the formation of this adduct have been carried out. Even though this process can occur *in vitro* catalyzed by manganese ion, the *in vivo* activation of INH requires KatG and in those KatG mutants identified as drug resistant, this process is thought to be inadequate or absent. A body of work appeared over the past several years in which the catalytic role of KatG was not clearly defined especially because of the addition of manganese in many experimental protocols. The added manganese is redox active in aerobic aqueous solutions and any Mn^{3+} formed is able to rapidly oxidize INH (54). A further complication arises because of the production of H_2O_2 in solutions in which dismutation of superoxide is facilitated by manganese redox activity.

The results presented here address issues concerning the role of hydrogen peroxide in the generation of the acyl-NAD molecule shown to be a potent inhibitor of InhA and considered responsible for the antibacterial function of the antibiotic, INH. We sought answers to a simple question: does hydrogen peroxide enhance the ability of KatG to produce the InhA acyl-NAD inhibitor molecule? Given the varied work that appears in the literature, including a widespread use of manganese in place of KatG or added in the presence of KatG, we considered this a worthwhile issue to investigate. We did not pursue any independent re-evaluation of the structure of the product or products generated in the reaction mixtures used here because prior literature clearly described the nature of the InhA inhibitor produced in oxidative reactions and their ability to inhibit InhA; we instead focused on the biomimetic aspects of the present approach.

We showed previously that INH at physiologically relevant concentrations reduces Compound I (35). Therefore, a continuous flow of H_2O_2 such as that in our experimental design here, which simulates the physiological environment in which drug activation and inhibition of InhA probably takes place, should stimulate drug function (Figure 4.8). Under such circumstances, we found that H_2O_2 can significantly improve the KatG catalyzed INH-NAD adduct production, especially when NADH is replace by NAD^+ and that removal of peroxidase intermediates in KatG interferes with generation of the adduct/inhibitor.

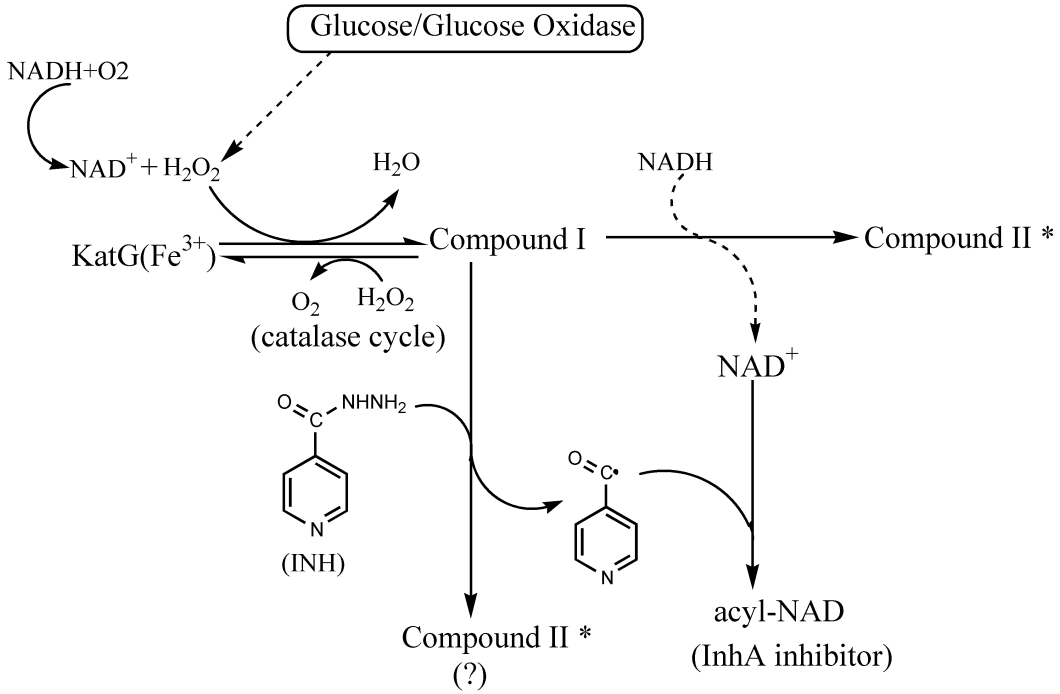

*: Not yet identified

Figure 4.8 Proposed mechanism of INH activation by KatG and hydrogen peroxide.

Other routes to initiate catalysis by KatG might include direct addition of superoxide to ferric KatG to produce Compound III; whether this is possible under conditions of infection is difficult to ascertain. *M. tuberculosis* has an SOD that is secreted and functions to dismutate superoxide to hydrogen peroxide, which would then be scavenged by KatG. Such reactions would still facilitate INH function according to the results in this chapter. Previous reports have shown that increasing superoxide flux in *M. smegmatis* renders bacteria more susceptible to INH (113). To completely understand the issue of in *vivo* INH activation would require knowledge about the relative abundance of the potential oxidants and the rates of their reaction with ferric KatG, and the relative rates of reaction of potential oxidizing forms of KatG with INH (Compound I, II, III). It is likely that the rate-limiting step for InhA inhibitor formation *in vivo*, given a constant ratio of NAD^+/NADH, is oxidation of INH. This reaction has been shown to generate radical intermediates (and possibly an acyl anion) that goes on to attack the nicotinamide ring of NAD^+ to form the covalent adduct (56,94-96).

Compound III was reported to be able to oxidize INH *in vitro*. Compound III could be produced under extraordinary conditions (such as in the presence of mM H_2O_2, or with a flux of superoxide generated by pulse radiolysis (60,114) but is unlikely to be available *in vivo* because physiological concentrations of H_2O_2 or superoxide don't approach those found to be required to produce Compound III *in vitro*.

In conclusion, our findings here are consistent with a low flux of hydrogen peroxide sustaining peroxidation of INH as a catalytic route to formation of the inhibitor of InhA designated as the target of drug action in mycobacteria.

CHAPTER 5

ACHIEVEMENTS AND FUTURE RESEARCH PLAN

During the last decade, *M. tuberculosis KatG* has become a hot subject within the research area of metallo-proteins. Provided with the extensive general characterization of this enzyme finished by previous investigators, my thesis research has been more focused on the catalytic mechanism of this enzyme, particularly in the context of INH activation.

To summarize, the accomplishment that I have made during the last five years includes the following:

1) Identification of tyrosyl radical formation on residue (Tyr 353) in KatG

2) Construction and characterization of KatG[Y353F] mutant enzyme which was also found to be able to form tyrosyl radical

3) Proposed and examined the function of hydrogen peroxide in the *in vitro* activation of INH by KatG and related it to the *in vivo* process. The obvious enhancing effect of H_2O_2 on the activation of INH has never been successfully demonstrated before. The progress we have made here is the mimicking of the *in vivo* cellular environment of *M. tuberculosis* by the introduction of a continuous flow of H_2O_2. This work also provided evidence that NAD^+, rather than NADH is the species that reacts with INH to form an InhA inhibitor.

4) Our collaboration with Dr. Sacchettini's group has led to successful crystallization and solution of the 3-dimensional structure of wild-type KatG and the KatG[S315T] mutant from drug resistant strains (unpublished as of this writing). The

formation of single crystal requires highly purified homogeneous protein. We achieved this goal by using multiple high-resolution FPLC columns. The crystal structure of S315T mutant was found to be very similar to that of wild type enzyme. The major difference is that in the mutant the bulky threonine residue blocked the channel through which the heme group is accessible to small molecules in wild type protein. This blockage might account for the reduced INH affinity in this mutant protein and as well as the origin of drug resistance.

Publications:

1. Zhao X., Yu H., Yu S., Wang F., Sacchetini J.C., Magliozzo R.S.
   Biomimetic approach to characterize the mechanism of INH activation by *M. tuberculosis* KatG. *In review.*

2. Zhao X., Girotto S., Yu S., Magliozzo R.S.
   Evidence for radical formation at Tyr-353 in *Mycobacterium tuberculosis* catalase-peroxidase (KatG). ***J. Biol. Chem***. 2004 Feb 27;279(9):7606-12.

3. Yu S., Girotto S., Zhao X., Magliozzo R.S.
   Rapid formation of compound II and a tyrosyl radical in the Y229F mutant of *Mycobacterium tuberculosis* catalase-peroxidase disrupts catalase but not peroxidase function. ***J. Biol. Chem***. 2003 Nov 7;278(45):44121-7

4. Kapetanaki S.M., Chouchane S., Yu S., Zhao X., Magliozzo R.S., Schelvis J.P.
   Mycobacterium tuberculosis KatG(S315T) catalase-peroxidase retains all active site properties for proper catalytic function. ***Biochemistry***. 2005 Jan 11;44(1):243-52.

Considering that the catalytic process of *M. tuberculosis* KatG is extremely complicated, more and more questions come up when dealing with the detailed pathways.

To gain more insight into how this enzyme behaves, further extensive investigation is needed. Following the work that I have finished, some interesting issues could be addressed in the future research:

1) Further follow the radical species involved in the catalytic cycle of KatG. If Y353 is mutated, what is the newly formed tyrosyl radical residue? Thus, similar labeling or trapping tests will help to reveal the new tyrosyl radical. Such study will also contribute to the description of this elaborate electron transportation chain possibly involved in a catalytic cycle independent of the heme intermediates.

2) Y229 is involved in a novel tri-amino acid adduct. When Y229 is mutated, this adduct was found broken by LC-Mass spectroscopy studies. Similar results were observed when two other residues (M255, W107) were mutated. In addition, the mutant enzymes lost most of their catalase activity. Have the broken triad changed the 3-dimensional structure of KatG? Moreover, how did this kind of structure change related to its catalase activity? Therefore, the determination of 3-d structure of any of Y229F, M255I, and W107F mutants will be of great help to elucidate the relationship of heme function and its surrounding structure. To date, crystallization of the KatG[229F] mutant has not been successful.

3) Several INH derivatives (benzoic acid hydrazide, furoic hydrazide, picolinic hydrazide, and nicotinic acid hydrazide) were found less potent as anti-tuberculosis agents. However, they also form similar adducts with INH when using manganese ions as catalyst (Wang F, U. of Texas A & M, personal communication). The structures of those adducts are all very similar. Thus, the difference in the bactericidal effect should

result from the *in vivo* activation process by KatG. Such hypothesis can be tested by our biomimetic method in the future to explain the role of KatG in INH function in detail.

APPENDIX A

MATERIALS AND METHODS

Materials:

Proline nonoate (PROLI/NO) was purchased from Cayman Chemical Company. Proteinase K, TPCK-treated trypsin, trifluoroacetic acid, 3-nitrotyrosine 2× crystallized bovine liver catalase, glucose oxidase (from A*spergillus niger*, low in catalase), NADH, INH, *o*-dianisidine and HPLC grade acetonitrile were all purchased from Sigma. LB and Glucose (enzyme grade) were purchased from Fisher Scientific. *trans*-2-dodecenoyl-CoA and InhA protein are a kind gift from Dr. James Sacchettini, Texas A & M University. All other chemicals were bought from Sigma-Aldrich with the highest purity grade available. Peroxyacetic acid (20%) was treated with catalase, as previously described, to remove hydrogen peroxide (50). INH was recrystallized from methanol and stored at 4 °C. All solutions of INH, β-NADH, β-NAD, and glucose were freshly made for all experiments.

Methods:

Chapters 2, 3

1. Quenching of tyrosyl radical by nitric oxide donor

Nitric oxide donor PROLI/NO (disodium 1-[2-(Carboxylato) pyrrolidin-1-yl] diazen-1-ium-1,2diolate) was dissolved in cold 10 mM NaOH immediately before use.

At neutral pH, decomposition of one mole PROLI/NO will yield two moles NO. The concentration of PROLI/NO stock solution was evaluated based on the absorbance at 252 nm (ε = 8400 $M^{-1} \cdot cm^{-1}$). For experiments designed to follow the quenching of the EPR signal of tyrosyl radical, 50 µl of 100 µM KatG solution (pH 7.2) was injected into an EPR tube followed by addition of 2 µl of 2.5 mM alkaline PROLI/NO. After one decomposition half-life (~2 s at pH 7.2 and 25 °C), 50 µl of 300 µM peroxyacetic acid (PAA) was added to initiate turnover of the resting (ferric) enzyme to Compound I, which is followed by tyrosyl radical formation (66). The samples were immediately immersed in liquid nitrogen and frozen. EPR spectra were subsequently recorded at 77 K using a Varian X-band spectrometer (66). Control experiments were performed under identical conditions, but without addition of PROLI/NO.

2. Protein nitration and HPLC analysis of nitrotyrosine-containing peptides

A molar ratio of KatG: PAA: PROLI/NO = 1: 6: 3 was used to get maximum yields of nitrated protein. Briefly, 150 µl of 100 µM KatG was mixed with a 3-fold excess of PROLI/NO in an Eppendorf tube; after 2 seconds of incubation at 37 °C, 150 µl PAA (600 µM) was added to the mixture. The resulting reaction mixture was incubated for 15 min at 37 °C. Ultrafiltration using a 30 kDa molecular weight cut-off Centricon centrifugal filter device (Millipore Corporation, Bedford, MA) was used to separate the enzyme from other components (5-washes of retentate with 2 ml 20 mM potassium phosphate buffer, pH 7.2).

Preliminary experiments were performed using Proteinase K for complete digestion of the NO-treated enzyme to ensure that optical detection of nitrotyrosine would not be compromised by interference from absorbance due to the presence of heme-

containing peptide(s). The 3 x ultra-filtered NO-treated KatG was subjected to proteolysis (in 20 mM potassium phosphate buffer, pH 7.2 at 37 °C for 16 hr) by the addition of 1:50 (w/w) Proteinase K. The digests were ultrafiltered (10 k-Da cut-off Microcon centrifugal filter device) prior to HPLC separation. Peptides were separated by reverse phase HPLC over a Zorbax SBC-18 column (4.6 X 250 mm). Buffer A was 0.1% TFA, and buffer B was 0.1% TFA in 80% acetonitrile. Elution was performed at a flow rate of 1.0 ml/min with a linear gradient from 0 to 60% B over 60 min, then 60% B to 100% B over 10 min followed by a series of washing steps. Absorbance was simultaneously monitored at 280 nm and 360 nm; the latter wavelength corresponds to an absorbance maximum of nitrotyrosine in acidic solution (115).

To further characterize peptides, fragments with strong absorbance at 360 nm were collected and dried using a Speed-Vac centrifuge and re-dissolved in either 0.1 N HCl or 0.1 N NaOH. UV-visible spectra were recorded using a 14NT UV-VIS spectrophotometer.

3. Construction, expression, and purification of the Y353F mutant of KatG

E. coli strain UM262 (*recA katG::*Tn*10 pro leu rpsL hsdM hsdR endl lacY*) (84) carrying pKatII was used for overexpression of both wild-type and mutated KatG proteins. pKatII plasmid containing cloned WT *katG* gene was extracted and purified from *E. coli* UM262 using *Wizard Plus Midipreps* DNA purification system form Promega (Madison, WI).

Pairs of complementary oligonucleotides:

5’-1043CTGGCGCTTGGCAAT**T**CACCGCCAAGGACGG1073-3’

5’-1073CCGTCCTTGGCGGTG**A**ATTGCCAAGCGCCAG1043-3’

(Synthesized and purified by Qiagene, CA) were designed to introduce the required mutation indicated in boldface to produce KatG[Y353F] (A to T mutation, Tyr-Phe replacement).

Mutagenesis was performed on pKatII using the QuickChange site-directed mutagenesis kit from Stratagene (La Jolla, CA) according to the manufacturer’s protocol. The PCR was performed using GeneAmp PCR System 2400(PERKIN ELMER) and the reaction products were transformed into the *E. coli* XL1-Blue strain (Stratagene) for selection and amplification. Plasmid was then extracted and purified from *E. coli* XL-Blue strain for sequencing.

Sequencing of the mutated *katG* gene was carried out by GeneWiz, Inc. When confirmed that only the desired nucleotide substitution was present, the mutated plasmid was transformed back into *E. coli* strain UM262 by electroporation for protein expression.

Overexpression and purification of mutant KatG[Y353F] were achieved as previously described for WT-KatG. Briefly, nine liters of liquid LB medium were inoculated with *E. coli* UM262 strain containing pKatII with the *katG* gene. Ampicillin was added to a final concentration of 1mg/ml to inhibit the growth of undesired bacteria. When $O.D._{600}$ reached 0.9-1.0, 20 μM of β-indolacrylic acid (previously dissolved in 95% ethanol) was added to induce the expression of KatG protein. At the same time, a heme precursor δ- aminolevulinic acid (200 μM final) was included to stimulate the *in vivo* synthesis of heme co-factor. After overnight growth at 28 ^{o}C with vigorous shaking (250 rpm), the cells were harvested by centrifugation. Following sonication in the

presence of protease inhibitor cocktail (Complete, from Roche Diagnostics, Inc.) and subsequent centrifugation, supernatant was collected and dialyzed against 20 mM phosphate buffer overnight.

The sample was then loaded onto an anion exchange column (FastQ, Amersham Biosciences) and eluted with a sodium chloride gradient in phosphate buffer The fractions with highest ratio (>0.1) of A405/A280 were saved and were subsequently treated with ammonium sulfate to 65% saturation. The precipitated protein was re-dissolved in phosphate buffer and loaded into a hydrophobic column (Phenyl Sepharose, Amersham Biosciences). Further purification was made by another high-resolution anion exchange column (MonoQ). To get rid of some small proteins, a gel filtration step (Superdex) was also employed to obtain highly purified protein.

4. Activity assay, catalase and peroxidase

Catalase activity: Catalase activity is assayed by following the disappearance of H_2O_2 at 240 nm. The O.D decrease is followed in 1.0 ml of solution containing 10mM potassium phosphate buffer pH=7.5, 25 mM H_2O_2 at 25^oC. KatG (1-5 µl) is added, and the absorbance followed at 240 nm (ε_{240nm} = 43.6 M^{-1} cm^{-1}). One unit of catalase activity is defined as the amount of enzyme catalyzing the decomposition of one µmol of H_2O_2/min at 25^oC.

Peroxidase activity: peroxidase activity is measured spectrophotometrically following the color development at 460nm. The enzyme assay (1ml) contains 23 mM ter-butylhydroperoxide, 0.1 mM *o*-dianisidine diHCl in 50 mM sodium acetate buffer pH=5.5. The enzyme (1-5µL) is added to the mixture at 25 ^oC and the absorbance

increase at 460nm is recorded (ε_{460}= 11.33 mM^{-1} cm^{-1}). One unit of peroxidase activity is defined as the amount of enzyme that catalyses formation of 1 μmole of product/min.

5. Rapid freeze quench study of Y353F mutant reacting with PAA

Rapid freeze-quench EPR samples were prepared as previously reported using a System 1000 Chemical/Freeze Quench Apparatus (Update Instrument, Inc.) (66). Specifically, wild type or mutant KatG (50 μM final) was mixed with three-fold excess peroxyacetic acid and aged for varying periods before freezing. Frozen samples were packed into quartz EPR tubes in an isopentane bath at -130 ^{o}C. EPR spectra were recorded at 77 K using a Bruker ElexSys E-500 EPR spectrometer operating at X-band. Spin quantitation was performed by double integration of EPR signals and comparison to a Cu(II)EDTA standard in 50% ethylene glycol also examined at 77 K. The dilution of KatG by isopentane in the frozen samples was also taken into account (66).

6. Optical stopped-flow spectrophotometry of KatG [Y353F]

Optical stopped-flow experiments were performed at 25 °C using a HiTech Scientific Model SF-61 DX2 apparatus equipped with a rapid scanning diode array spectrophotometer as previously published (35). The final concentrations of KatG[Y353F] mutant enzyme (50μM) and PAA (150μM) were the same as those used in the RFQ-EPR studies.

Chapter 4

1. Inhibition of InhA

InhA (1.0 μM) was incubated with KatG or KatG[S315T] mutant (0.5 μM), NADH (50 μM) and isoniazid (50 μM) in a total volume of 1.0 ml, at 25 ºC in 20 mM phosphate buffer, pH 7.2. Glycerol (8% v/v) and bovine serum albumin (0.1 mg/ml) were also included to stabilize InhA. Aliquots (30 μl) were taken at defined time points and residual InhA activity was measured in a spectrophotometric assay following the loss of absorbance of NADH at 340 nm using 2-*trans*-dodecenoyl-CoA (100 μM) and excess NADH (200 μM) as substrates added to initiate the assay reaction. Specific activity was calculated as μmoles NADH ($\varepsilon_{340} = 6220\ M^{-1}\ cm^{-1}$) oxidized per minute per mg of InhA. The InhA residual activity at various time points was expressed relative to 100%, which is the value measured at time zero for an aliquot removed from the reaction mixture immediately after mixing.

2. Effects of catalase and o-dianisidine on the adduct/inhibitor production

Varying amounts of commercial bovine liver catalase (0.25 or 0.5 μM) or *o*-dianisidine (20 or 200 μM) were added directly to reaction mixtures containing KatG, INH, NADH, and InhA as described above. The InhA residual activity was measured accordingly in aliquots removed at defined time points as above.

3. Effects of enzymatically generated H_2O_2 on adduct/inhibitor generation

H_2O_2 was generated using a glucose /glucose oxidase (G/GOx) system. GOx (2 or 10 mU), together with 5 mM glucose, were added to the reaction mixtures containing KatG, INH, NADH and InhA. Residual InhA activities were measured in aliquots removed at defined time points. The rate of hydrogen peroxide release by the G/GOx

system was determined separately. Briefly, glucose (5 mM) and horseradish peroxidase (50 μg/ml) were added to 1.0 ml of 20 mM phosphate buffer, containing 1% *o*-dianisidine, pH 7.2. The reaction (production of hydrogen peroxide at the expense of oxygen in solution) was started by the addition of glucose oxidase (2 or 10 mU) and the oxidation of *o*-dianisidine was monitored by the increase in absorbance at 460 nm (ε_{460} = 11.33 mM^{-1} cm^{-1}). The μmoles of *o*-dianisidine oxidized correspond to μmoles of H_2O_2 produced by G/GOx. Oxygen concentration in air-saturated solutions is greater than 0.2 mM, a large excess relative to the rate of turnover of the oxidase.

4. Trapping of INH-NAD adduct by InhA

The inhibitor generated in reaction mixtures containing INH, NAD, KatG, and GOx/glucose in the absence of InhA was isolated according to Lei et al. (59) with minor modification. Briefly, 1.0 ml of 20 mM phosphate buffer (pH 7.2) containing KatG (1 μM), INH (200 μM), NAD (200 μM), Gox (40 mU), and glucose (5 mM) was incubated aerobically at room temperature for 50 min. The reaction was terminated by the removal of KatG and GOx through ultrafiltration using a 30-kDa cut-off filter. A portion of the filtrate (850 μl) was mixed with 50 μl of 600 μM InhA and incubated at room temperature for 20 min to ensure equilibration of InhA with inhibitor. The InhA-inhibitor complex was isolated by gel filtration on a Sephadex G-25 column (1 × 60 cm) previously equilibrated in 20 mM potassium phosphate buffer, pH 7.2. The flow rate was 0.25 ml/min. Fractions containing InhA were collected and concentrated to a final volume of 1.0 ml. The UV-visible spectrum was subsequently recorded with a 14NT UV-visible spectrophotometer (AVIV Biomedical, Inc.). This type of procedure had

been shown elsewhere (58,59) to allow recovery of the InhA-inhibitor complex, which is very stable.

5. INH and NAD concentration dependence of INH-NAD formation

The rates of INH-NAD adduct generation with varying concentrations of INH were examined directly with either KatG or KatG[S315T] mutant in a spectrophotometric assay. This study was carried out in the absence of InhA, using KatG (0.5 μM), NAD^+ (50 μM), GOx (10 mU/ml), and glucose (5 mM). Free NAD^+ shows no absorbance at 326 nm, which is a characteristic absorbance peak of the acyl-NAD molecule. The generation of adduct was initiated by the addition of varying amounts of INH (5, 10, 20, 30, and 50 μM). In the case of KatG[S315T] mutant, higher concentrations of INH (0.25, 0.5, 1, and 2 mM) were required to achieve detectable increases in absorbance in reasonable time periods. To monitor the adduct formation, the absorbance at 326 nm was recorded for 20 min after the addition of INH. The reference cuvette contained all components except NAD^+ to correct for background.

The study of the NAD^+ dependence of adduct formation was carried out similarly by varying the amount of NAD^+ (25, 50, 100, 200 μM), the concentrations of other components are fixed as following: KatG (0.5 μM), INH (50 μM), GOx (10 mU/ml), and glucose (5 mM).

APPENDIX B

Amino acid sequence of *M. tuberculosis* KatG (from strain H37Rv)

```
  1 MPEQHPPITE TTTGAASNGC PVVGHMKYPV EGGGNQDWWP NRLNLKVLHQ NPAVADPMGA
 61 AFDYAAEVAT IDVDALTRDI EEVMTTSQPW WPADYGHYGP LFIRMAWHAA GTYRIHDGRG
121 GAGGGMQRFA PLNSWPDNAS LDKARRLLWP VKKKYGKKLS WADLIVFAGN CALESMGFKT
181 FGFGFGRVDQ WEPDEVYWGK EATWLGDERY SGKRDLENPL AAVQMGLIYV NPEGPNGNPD
241 PMAAAVDIRE TFRRMAMNDV ETAALIVGGH TFGKTHGAGP ADLVGPEPEA APLEQMGLGW
301 KSSYGTGTGK DAITSGIEVV WTNTPTKWDN SFLEILYGYE WELTKSPAGA WQYTAKDGAG
361 AGTIPDPFGG PGRSPTMLAT DLSLRVDPIY ERITRRWLEH PEELADEFAK AWYKLIHRDM
421 GPVARYLGPL VPKQTLLWQD PVPAVSHDLV GEAEIASLKS QIRASGLTVS QLVSTAWAAA
481 SSFRGSDKRG GANGGRIRLQ PQVGWEVNDP DGDLRKVIRT LEEIQESFNS AAPGNIKVSF
541 ADLVVLGGCA AIEKAAKAAG HNITVPFTPG RTDASQEQTD VESFAVLEPK ADGFRNYLGK
601 GNPLPAEYML LDKANLLTLS APEMTVLVGG LRVLGANYKR LPLGVFTEAS ESLTNDFFVN
661 LLDMGITWEP SPADDGTYQG KDGSGKVKWT GSRVDLVFGS NSELRALVEV YGADDAQPKF
721 VQDFVAAWDK VMNLDRFDVR
```

BIBLIOGRAPHY

1. Zimmerman, M. R. (1979) *Bull. N. Y. Acad. Med.* **55**(6), 604-608

2. Nerlich, A. G., Haas, C. J., Zink, A., Szeimies, U., and Hagedorn, H. G. (1997) *Lancet* **350**(9088), 1404

3. Bloom, B. R., and Murray, C. J. (1992) *Science* **257**(5073), 1055-1064

4. WHO. (1999) World Health Report. In., World Health Organization, Geneva

5. Iseman, M. D. (1999) *Chemotherapy* **45**(Suppl.2), 34-40

6. Raviglione, M. C., Harries, A. D., Msiska, R., Wilkinson, D., and Nunn, P. (1997) *Aids* **11 Suppl. B**, S115-123

7. Grange, J. M., Gibson, J., Osborn, T. W., Collins, C. H., and Yates, M. D. (1983) *Tubercle.* **64**(2), 129-139

8. Smith, P. G., Rodrigues, L. C., and Fine, P. E. (1984) *Int. J. Epidemiol.* **13**(1), 87-93

9. Corper, H. J., and Cohn, M. L. (1952) *Acta. Tuberc. Scand.* **26**(1-2), 92-95

10. Chorine, S. V. (1945) *Comp. Rend. Acad. Sci.* **220**, 150

11. Pansy, F., Stander, H., and Donovick, R. (1952) *Am. Rev. Tuberc.* **65**(6), 761-764

12. Wolinsky, E. (1992) *Clin. Infect. Dis.* **15**(1), 1-10

13. Fox, W., and Mitchison, D. A. (1975) *Am. Rev. Respir. Dis.* **111**(6), 845-848 CONTD

14. Takayama, K., Wang, L., and David, H. L. (1972) *Antimicrob. Agents. Chemother.* **2**(1), 29-35

15. Takayama, K., Wang, L., and Merkal, R. S. (1973) *Antimicrob. Agents Chemother.* **4**(1), 62-65

16. Quemard, A., Lacave, C., and Laneelle, G. (1991) *Antimicrob. Agents Chemother.* **35**(6), 1035-1039

17. Davidson, L. A., and Takayama, K. (1979) *Antimicrob. Agents Chemother.* **16**(1), 104-105

18. Somoskovi, A., Parsons, L. M., and Salfinger, M. (2001) *Respir. Res.* **2**(3), 164-168

19. Banerjee, A., Dubnau, E., Quemard, A., Balasubramanian, V., Um, K. S., Wilson, T., Collins, D., de Lisle, G., and Jacobs, W. R., Jr. (1994) *Science* **263**(5144), 227-230

20. Quemard, A., Sacchettini, J. C., Dessen, A., Vilcheze, C., Bittman, R., Jacobs, W. R., Jr., and Blanchard, J. S. (1995) *Biochemistry* **34**(26), 8235-8241

21. Dessen, A., Quemard, A., Blanchard, J. S., Jacobs, W. R., Jr., and Sacchettini, J. C. (1995) *Science* **267**(5204), 1638-1641

22. Mdluli, K., Slayden, R. A., Zhu, Y., Ramaswamy, S., Pan, X., Mead, D., Crane, D. D., Musser, J. M., and Barry, C. E., 3rd. (1998) *Science* **280**(5369), 1607-1610

23. Slayden, R. A., Lee, R. E., and Barry, C. E., 3rd. (2000) *Mol. Microbiol.* **38**(3), 514-525.

24. Middlebrook, G., and Cohn, M. L. (1953) *Science* **118**, 297-299

25. Middlebrook, G. (1954) *Am. Rev. Tuberc.* **69**(3), 471-472

26. Dunbar, F. P., Mc, A. E., and Jefferies, M. B. (1959) *Am. Rev. Tuberc.* **79**(5), 669-671

27. Zhang, Y., Heym, B., Allen, B., Young, D., and Cole, S. (1992) *Nature* **358**(6387), 591-593

28. Zhang, Y., Garbe, T., and Young, D. (1993) *Mol. Microbiol.* **8**(3), 521-524.

29. Heym, B., Honore, N., Truffot-Pernot, C., Banerjee, A., Schurra, C., Jacobs, W. R., Jr., van Embden, J. D., Grosset, J. H., and Cole, S. T. (1994) *Lancet* **344**(8918), 293-298

30. Rouse, D. A., Li, Z., Bai, G. H., and Morris, S. L. (1995) *Antimicrob. Agents Chemother.* **39**(11), 2472-2477

31. Wilson, T. M., de Lisle, G. W., and Collins, D. M. (1995) *Mol. Microbiol.* **15**(6), 1009-1015

32. Cockerill, F. R., 3rd, Uhl, J. R., Temesgen, Z., Zhang, Y., Stockman, L., Roberts, G. D., Williams, D. L., and Kline, B. C. (1995) *J. Infect. Dis.* **171**(1), 240-245

33. Heym, B., Alzari, P. M., Honore, N., and Cole, S. T. (1995) *Mol. Microbiol.* **15**(2), 235-245

34. Johnsson, K., Froland, W. A., and Schultz, P. G. (1997) *J. Biol. Chem.* **272**(5), 2834-2840

35. Chouchane, S., Lippai, I., and Magliozzo, R. S. (2000) *Biochemistry* **39**(32), 9975-9983

36. Marcinkeviciene, J. A., Magliozzo, R. S., and Blanchard, J. S. (1995) *J. Biol. Chem.* **270**(38), 22290-22295

37. Johnsson, K., King, D. S., and Schultz, P. G. (1995) *J. Am. Chem. Soc.* **117**(17), 5009-5010

38. Pym, A. S., Domenech, P., Honore, N., Song, J., Deretic, V., and Cole, S. T. (2001) *Mol. Microbiol.* **40**(4), 879-889.

39. Zhang, Y., and Young, D. B. (1993) *Trends Microbiol.* **1**(3), 109-113.

40. Dunford, H. B. (1999) *Heme peroxidases*, John Wiley, New York

41. Welinder, K. G. (1991) *Biochim. Biophys. Acta* **1080**(3), 215-220

42. Yamada, Y., Fujiwara, T., Sato, T., Igarashi, N., and Tanaka, N. (2002) *Nat. Struct. Biol.* **9**(9), 691-695

43. Carpena, X., Loprasert, S., Mongkolsuk, S., Switala, J., Loewen, P. C., and Fita, I. (2003) *J. Mol. Biol.* **327**(2), 475-489

44. Bertrand, T., Eady, N. A., Jones, J. N., Jesmin, Nagy, J. M., Jamart-Gregoire, B., Raven, E. L., and Brown, K. A. (2004) *J. Biol. Chem.* **279**(37), 38991-38999

45. Nagy, J. M., Cass, A. E., and Brown, K. A. (1997) *J. Biol. Chem.* **272**(50), 31265-31271

46. Kapetanaki, S., Chouchane, S., Girotto, S., Yu, S., Magliozzo, R. S., and Schelvis, J. P. (2003) *Biochemistry* **42**(13), 3835-3845

47. Jakopitsch, C., Kolarich, D., Petutschnig, G., Furtmuller, P. G., and Obinger, C. (2003) *FEBS Lett.* **552**(2-3), 135-140

48. Jakopitsch, C., Auer, M., Ivancich, A., Ruker, F., Furtmuller, P. G., and Obinger, C. (2003) *J. Biol. Chem.* **278**(22), 20185-20191

49. Regelsberger, G., Jakopitsch, C., Furtmuller, P. G., Rueker, F., Switala, J., Loewen, P. C., and Obinger, C. (2001) *Biochem. Soc. Trans.* **29**(Pt 2), 99-105.

50. Yu, S., Girotto, S., Zhao, X., and Magliozzo, R. S. (2003) *J. Biol. Chem.* **278**(45), 44121-44127

51. Dunford, H. B. (1991) Horseradish Peroxidase: Structure and Kinetic Properties. In: Everse, J., Everse, K. E., and Grisham, M. B. (eds). *Peroxidases in chemistry and biology*, CRC Press, Boca Raton, Fla.

52. Schulz, C. E., Devaney, P. W., Winkler, H., Debrunner, P. G., Doan, N., Chiang, R., Rutter, R., and Hager, L. P. (1979) *FEBS Lett.* **103**(1), 102-105.

53. Scheeline, A., Olson, D. L., Williksen, E. P., Horras, G. A., Klein, M. L., and Larter, R. (1997) *Chem. Rev.* **97**(3), 739-756

54. Magliozzo, R. S., and Marcinkeviciene, J. A. (1997) *J. Biol. Chem.* **272**(14), 8867-8870

55. Singh, R., Wiseman, B., Deemagarn, T., Donald, L. J., Duckworth, H. W., Carpena, X., Fita, I., and Loewen, P. C. (2004) *J. Biol. Chem.* **279**(41), 43098-43106

56. Johnsson, K., and Schultz, P. G. (1994) *J. Am. Chem. Soc.* **116**, 7425-7426

57. Rozwarski, D. A., Grant, G. A., Barton, D. H., Jacobs, W. R., Jr., and Sacchettini, J. C. (1998) *Science* **279**(5347), 98-102

58. Rawat, R., Whitty, A., and Tonge, P. J. (2003) *Proc. Natl. Acad. Sci. U S A* **100**(24), 13881-13886

59. Lei, B., Wei, C. J., and Tu, S. C. (2000) *J. Biol. Chem.* **275**(4), 2520-2526

60. Ghiladi, R. A., Cabelli, D. E., and Ortiz de Montellano, P. R. (2004) *J. Am. Chem. Soc.* **126**(15), 4772-4773

61. Unkrig, V., Neugebauer, F. A., and Knappe, J. (1989) *Eur. J. Biochem.* **184**(3), 723-728.

62. Licht, S., Gerfen, G. J., and Stubbe, J. (1996) *Science* **271**(5248), 477-481

63. Barry, B. A., el-Deeb, M. K., Sandusky, P. O., and Babcock, G. T. (1990) *J. Biol. Chem.* **265**(33), 20139-20143.

64. McIntire, W. S., Wemmer, D. E., Chistoserdov, A., and Lidstrom, M. E. (1991) *Science* **252**(5007), 817-824

65. Stubbe, J., and Donk, W. A. v. d. (1998) *Chem. Rev.* **98**(2), 705 -762

66. Chouchane, S., Girotto, S., Yu, S., and Magliozzo, R. S. (2002) *J. Biol. Chem.* **277**(45), 42633-42638

67. Tsai, A., Wu, G., Palmer, G., Bambai, B., Koehn, J. A., Marshall, P. J., and Kulmacz, R. J. (1999) *J. Biol. Chem.* **274**(31), 21695-21700

68. Tsai, A., and Kulmacz, R. J. (2000) *Prostaglandins Other Lipid Mediat.* **62**(3), 231-254

69. Gunther, M. R., Sturgeon, B. E., and Mason, R. P. (2000) *Free Radic. Biol. Med.* **28**(5), 709-719.

70. Tang, X. S., Chisholm, D. A., Dismukes, G. C., Brudvig, G. W., and Diner, B. A. (1993) *Biochemistry* **32**(49), 13742-13748.

71. Ivancich, A., Jouve, H. M., Sartor, B., and Gaillard, J. (1997) *Biochemistry* **36**(31), 9356-9364

72. Ivancich, A., Mazza, G., and Desbois, A. (2001) *Biochemistry* **40**(23), 6860-6866.

73. Chen, Y. R., Gunther, M. R., and Mason, R. P. (1999) *J. Biol. Chem.* **274**(6), 3308-3314.

74. Karthein, R., Dietz, R., Nastainczyk, W., and Ruf, H. H. (1988) *Eur. J. Biochem.* **171**(1-2), 313-320.

75. Tsai, A., Hsi, L. C., Kulmacz, R. J., Palmer, G., and Smith, W. L. (1994) *J. Biol. Chem.* **269**(7), 5085-5091

76. Lepoivre, M., Flaman, J. M., Bobe, P., Lemaire, G., and Henry, Y. (1994) *J. Biol. Chem.* **269**(34), 21891-21897

77. Eiserich, J. P., Butler J., Van der Vliet A., Cross, C. E., and Halliwell, B. (1995) *Biochem. J.* **310**, 745-749

78. Lepoivre, M., Fieschi, F., Coves, J., Thelander, L., and Fontecave, M. (1991) *Biochem. Biophys. Res. Commun.* **179**(1), 442-448

79. Gunther, M. R., Hsi, L. C., Curtis, J. F., Gierse, J. K., Marnett, L. J., Eling, T. E., and Mason, R. P. (1997) *J. Biol. Chem.* **272**(27), 17086-17090

80. Goodwin, D. C., Gunther, M. R., Hsi, L. C., Crews, B. C., Eling, T. E., Mason, R. P., and Marnett, L. J. (1998) *J. Biol. Chem.* **273**(15), 8903-8909.

81. Sivaraja, M., Goodin, D. B., Smith, M., and Hoffman, B. M. (1989) *Science* **245**(4919), 738-740.

82. Hiner, A. N. P., Martinez, J. I., Arnao, M. B., Acosta, M., Turner, D. D., Lloyd Raven, E., and Rodriguez-Lopez, J. N. (2001) *Eur. J. Biochem.* **268**(10), 3091-3098

83. Morimoto, A., Tanaka, M., Takahashi, S., Ishimori, K., Hori, H., and Morishima, I. (1998) *J. Biol. Chem.* **273**(24), 14753-14760

84. Loewen, P. C., Switala, J., Smolenski, M., and Triggs-Raine, B. L. (1990) *Biochem. Cell Biol.* **68**(7-8), 1037-1044

85. Blodig, W., Smith, A. T., Doyle, W. A., and Piontek, K. (2001) *J. Mol. Biol.* **305**(4), 851-861

86. Blodig, W., Smith, A. T., Winterhalter, K., and Piontek, K. (1999) *Arch. Biochem. Biophys.* **370**(1), 86-92

87. Girotto, S. (2004) Application of EPR spectroscopy to study the resting state structure and the mechanism of *Mycobacterium tuberculosis* catalase-peroxidase (KatG). In. *Ph.D thesis*, The City University of New York, New York

88. Jakopitsch, C., Ivancich, A., Schmuckenschlager, F., Wanasinghe, A., Poltl, G., Furtmuller, P. G., Ruker, F., and Obinger, C. (2004) *J. Biol. Chem.* **279**(44), 46082-46095

89. Wengenack, N. L., Uhl, J. R., St Amand, A. L., Tomlinson, A. J., Benson, L. M., Naylor, S., Kline, B. C., Cockerill, F. R., 3rd, and Rusnak, F. (1997) *J. Infect. Dis.* **176**(3), 722-727.

90. Saint-Joanis, B., Souchon, H., Wilming, M., Johnsson, K., Alzari, P. M., and Cole, S. T. (1999) *Biochem. J.* **338**, 753-760

91. Wengenack, N. L., Todorovic, S., Yu, L., and Rusnak, F. (1998) *Biochemistry* **37**(45), 15825-15834

92. Yu, S., Girotto, S., Lee, C., and Magliozzo, R. S. (2003) *J. Biol. Chem.* **278**(17), 14769-14775

93. Wei, C. J., Lei, B., Musser, J. M., and Tu, S. C. (2003) *Antimicrob. Agents Chemother.* **47**(2), 670-675

94. Wilming, M., and Johnsson, K. (1999) *Angew Chem. Int. Ed. Engl.* **38**(17), 2588-2590

95. Nguyen, M., Quemard, A., Broussy, S., Bernadou, J., and Meunier, B. (2002) *Antimicrob. Agents Chemother.* **46**(7), 2137-2144.

96. Nguyen, M., Claparols, C., Bernadou, J., and Meunier, B. (2001) *Chembiochem* **2**(12), 877-883

97. Magliozzo, R. S., and Marcinkeviciene, J.A. (1996) *J. Am. Chem. Soc.* **118**, 11303-11304

98. Zhao, X., Girotto, S., Yu, S., and Magliozzo, R. S. (2004) *J. Biol. Chem.* **279**(9), 7606-7612

99. Yokota, K., and Yamazaki, I. (1977) *Biochemistry* **16**(9), 1913-1920

100. Gonzalez-Flecha, B., and Demple, B. (1997) *J. Bacteriol.* **179**(2), 382-388

101. Musser, J. M. (1996) *Emerg. Infect. Dis.* **2**(1), 1-17

102. Victor, T. C., Pretorius, G. S., Felix, J. V., Jordaan, A. M., van Helden, P. D., and Eisenach, K. D. (1996) *Antimicrob. Agents Chemother.* **40**(6), 1572

103. Michan, C., Manchado, M., Dorado, G., and Pueyo, C. (1999) *J. Bacteriol.* **181**(9), 2759-2764

104. Schellhorn, H. E. (1995) *FEMS Microbiol. Lett.* **131**(2), 113-119

105. Sherman, D. R., Sabo, P. J., Hickey, M. J., Arain, T. M., Mahairas, G. G., Yuan, Y., Barry, C. E., 3rd, and Stover, C. K. (1995) *Proc. Natl. Acad. Sci. U S A* **92**(14), 6625-6629

106. Master, S., Zahrt, T. C., Song, J., and Deretic, V. (2001) *J. Bacteriol.* **183**(13), 4033-4039

107. Collins, D. M. (1996) *Trends Microbiol.* **4**(11), 426-430

108. Mariani, F., Cappelli, G., Riccardi, G., and Colizzi, V. (2000) *Gene* **253**(2), 281-291

109. Ng, V. H., Cox, J. S., Sousa, A. O., MacMicking, J. D., and McKinney, J. D. (2004) *Mol. Microbiol.* **52**(5), 1291-1302

110. Rosner, J. L., and Storz, G. (1994) *Antimicrob. Agents Chemother.* **38**(8), 1829-1833

111. Miesel, L., Weisbrod, T. R., Marcinkeviciene, J. A., Bittman, R., and Jacobs, W. R., Jr. (1998) *J. Bacteriol.* **180**(9), 2459-2467

112. Vilcheze, C., Weisbrod, T. R., Chen, B., Kremer, L., Hazbon, M. H., Wang, F., Alland, D., Sacchettini, J. C., and Jacobs, W. R., Jr. (2005) *Antimicrob. Agents Chemother.* **49**(2), 708-720

113. Wang, J. Y., Burger, R. M., and Drlica, K. (1998) *Antimicrob. Agents Chemother.* **42**(3), 709-711

114. Wengenack, N. L., Hoard, H.M., Rusnak, F. (1999) *J. Am. Chem. Soc.* **121**, 9748-9749

115. Packer, L. (1996) *Methods Enzymol.* **269**, 185-194